Hindawi Publishing Corporation
Advances in Chemistry
Volume 2015, Article ID 463874, 21 pages
http://dx.doi.org/10.1155/2015/463874

Review Article

Optical Breakdown in Liquid Suspensions and Its Analytical Applications

Tatiana Kovalchuk-Kogan, Valery Bulatov, and Israel Schechter

Schulich Department of Chemistry, Technion, Israel Institute of Technology, 32000 Haifa, Israel

Correspondence should be addressed to Israel Schechter; israel@techunix.technion.ac.il

Received 4 November 2014; Accepted 10 January 2015

Academic Editor: Armando Zarrelli

Micro- and nanoparticles persist in all environmental aquatic systems and their identification and quantification are of considerable importance. Therefore, the application of Laser-induced breakdown to aquatic particles is of interest. Since direct application of this method to water samples is difficult, further understanding of the breakdown is needed. We describe several optical techniques for investigation of laser breakdown in water, including Mach-Zehnder interferometry, shadow, and Schlieren diagnostic. They allow for studying the time dependent structure and physical properties of the breakdown at high temporal and spatial resolutions. Monitoring the formation of microbubbles, their expansion, and the evolution of the associated shockwaves are described. The new understanding is that the plasma column in liquids has a discrete nature, which lasts up to 100 ns. Controlling the generation of nanoparticles in the irradiated liquids is discussed. It is shown that multivariate analysis of laser-induced breakdown spectroscopy allows for differentiation between various groups of suspended particulates.

This review is dedicated to the memory of Gregory Toker, a devoted scientist who had major contributions to the field of optical breakdown and its investigation using interferometric techniques, who passed away during the preparation of this review

1. Liquid Suspensions

The effect of micro- and nanoparticles on migration of pollutants is a major environmental concern [1]. Micro- and nanoparticles are present in all aquatic systems [1–4]. The characteristic particle sizes are between 1 nm and 10 μm and they possess a high surface to mass ratio. Sorption of contaminants on their surfaces can result in severe pollution. In addition, micro- and nanoparticles may provide a medium for microbial growth. The common waterborne particulates include the following:

(a) mineral particles: clay, silica, hydroxides, and metallic salts;

(b) organic particles: humic and fulvic acids stemming from the decomposition of vegetable and animal matter;

(c) biological particles: microorganisms such as pollens, bacteria, plankton, algae, and viruses.

Besides the environmental effects, waterborne particles are often unwanted contaminants in industrial processes, since they often reduce the product quality [5]. Therefore the development of fast and simple methods for characterization of particles in water is of considerable importance. There are several known methods for detection of particles in water [5] but laser-induced breakdown detection (LIBD) is one of the most promising experimental techniques for direct quantification of aquatic colloids.

LIBD has the potential to provide online analysis of particles in water. Therefore understanding the breakdown mechanism in water is of considerable importance. In principle, LIBD is based on generation of discharge events induced by a laser at colloidal particles [6]. In this method, a high power laser pulse is focused in a sample, thus generating a local plasma or laser spark. The emission from the atoms and ions in the plasma is collected by an optic fiber and guided to a detector. LIBD involves the collection and processing of the spectral signature resulting from the plasma and the analytes

[7]. The generic nature of the breakdown has been utilized as a robust and conceptually simple method for elemental characterization of gases [8], solids [9], and aerosols [7, 10, 11].

When suspensions are concerned, LIBD is capable of detecting very small particulates, even at low concentrations [12–17]. However, the currently available methods suffer from considerable difficulties associated with quantification of particles in water [5, 13]. In this environment, particles of diameter smaller than 100 nm can be detected only at relatively high concentrations.

2. Laser Breakdown in Liquids

The interaction of high intensity light with condensed matter leads to breakdown. The origin of breakdown in air has been investigated [18], as well as the characteristics of the breakdown process itself [19]. The process requires high power densities of about 10^8 W cm^{-2}. Such power densities can be produced by focusing a pulsed laser beam of a few mJ and several ns pulse duration [12, 20]. As a result, the electrons are released from atoms and molecules by a multiphoton absorption avalanche mechanism. The initially released electrons are accelerated in the electric field of the laser pulse. Electron avalanche is produced by the electrons which knock out other electrons from the atoms and molecules. During the plasma generation process, the plasma heats up by several thousand Kelvins and its volume expands by creating a shockwave. The plasma is eventually cooled down by emission of light and other processes. Figure 1 represents the generation of plasma in liquids.

The breakdown energy threshold is the minimum energy density required for plasma generation and depends on the state of aggregation of the medium. It is highest for gases, lower for liquids, and lowest for solids [21]. Often the medium density (liquids and solids) can be modified for improved LIBD. For example, when the laser energy is not sufficient for inducing breakdown in pure water, addition of particles can solve the problem.

3. Visualization Techniques for Optical Breakdown

First experiments on visualizing the region of laser breakdown have been performed in gaseous atmosphere [22, 23]. Studying the optical breakdown has been carried out in the microsecond and partially in nanosecond ranges, by applying coherent and noncoherent techniques [24–28]. The morphology of breakdown on surfaces was also investigated in detail, using several technologies [29, 30]. Breakdown in water in picosecond and femtosecond temporal ranges has also been investigated [20, 31, 32]. However, studying the discrete character of breakdown events requires better spatial resolution than was done in the past. The following three methods are especially suited for visualization of breakdown processes in water: shadowgraphy, Schlieren, and Mach-Zehnder interferometry.

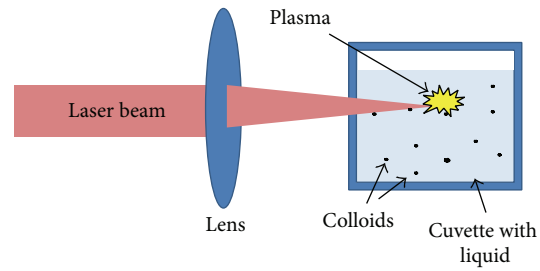

Figure 1: Schematic illustration of breakdown generation in liquid.

3.1. Shadowgraphy. Shadowgraphy is an optical technique that reveals nonuniformities in transparent media such as air, water, or glass [33–42]. Regular vision and optical inspection methods are not sensitive to temperature differences, to variations in gas composition, or to shockwaves in air. However, these disturbances refract light, so they can cast shadows. A point (or collimated) light source is used for direct illumination of the transparent object under study. The phase of the diagnostic wave can be changed by warm air or other events that cause nonhomogeneity in the medium. This phase change causes shadows on the screen.

Applications of shadowgraphy in science and technology are very broad. It is used in aerospace engineering to visualize the flow about high-speed aircrafts and missiles, as well as in combustion research, ballistics, and explosions and in testing of glass quality. A shadowgram (the result of applying the shadowgraphic technique) is not a focused image; rather it is a mere shadow. In a shadowgram, the differences in light intensities are proportional to the second spatial derivative of the refractive index field in the transparent medium under study.

3.2. Schlieren Technique. The basic optical Schlieren system uses light from a collimated source. Variations in refractive index caused by density gradients in the fluid distort the collimated light beam. This distortion creates a spatial variation in the intensity of the light, which can be visualized directly by using optical diaphragms [33–42].

In Schlieren photography, the collimated light is focused on a knife-edge obstacle (the so-called Foucault knife) placed in the focal plane, so that the source image is projected onto the edge of the knife. If the sample contains no density gradients or other optical inhomogeneities, the light is blocked by that obstacle. Otherwise, a part of the light is scattered and passes above the barrier and forms an image on the detector.

The result is a set of lighter and darker patches corresponding to positive and negative density gradients in the direction normal to the knife-edge. This system measures the first derivative of density in the direction perpendicular to the knife-edge. Schlieren method provides a high contrast image.

An experimental setup representing the application of Schlieren technique to breakdown in liquids is shown in Figure 2. In this setup, the optical collimation system sharply focused the breakdown region onto the imaging detector.

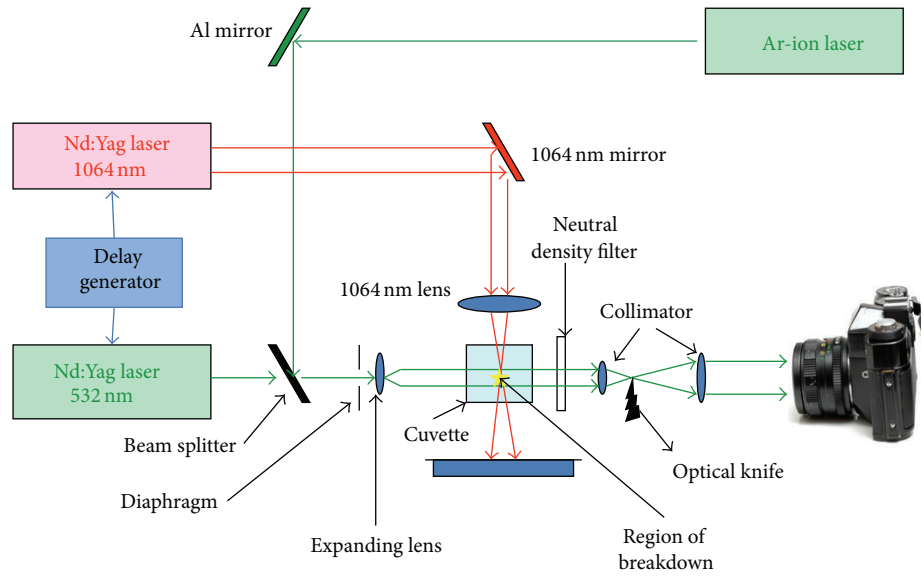

Figure 2: Experimental setup for Schlieren technique and its application to breakdown in liquid suspensions.

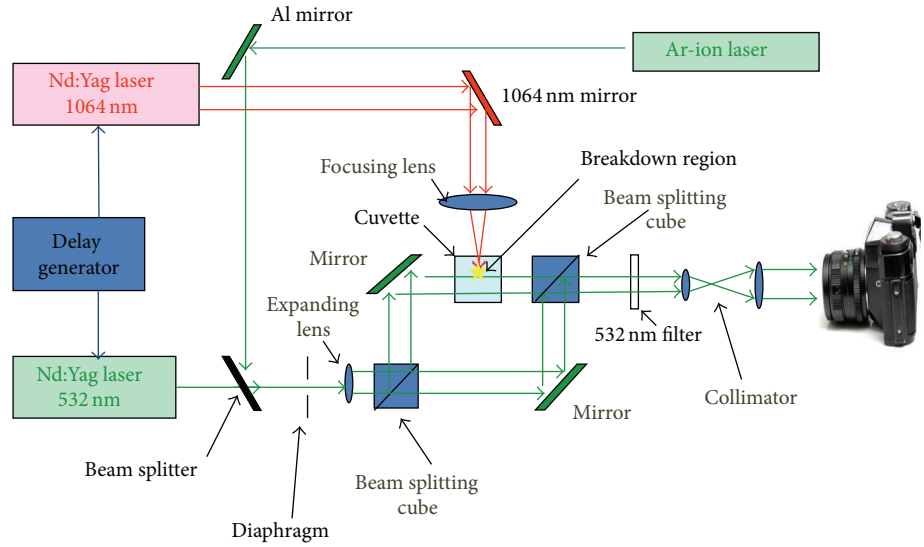

Figure 3: Experimental setup for application of Mach-Zehnder interferometry to breakdown in liquids.

In this setup the plasma was initiated by a Nd:YAG laser (λ = 1064 nm, 6 ns), which was focused into a quartz-windowed cuvette, where the liquid under study was located. A second laser (2nd harmonic of a Nd:YAG) was used for probing the cuvette in a direction perpendicular to the first laser beam. The probing laser was fired at controllable time delay after the first laser pulse, such that time-resolved information can be achieved. An argon-ion laser was used for alignment and adjustment of the optical components.

3.3. Mach-Zehnder Interferometry. Mach-Zehnder interferometer is a device used to determine the phase shift caused by a small sample which is placed in the path of one of two collimated beams (thus having plane wave fronts) from a coherent light source [33–42]. A collimated beam is split by a half-silvered mirror. The two resulting beams (the "sample beam" and the "reference beam") are each reflected by a mirror. The two beams then pass a second half-silvered mirror. Reflection at the surface of a medium with a higher refractive index causes a phase shift. Mach-Zehnder interferometer has two important features. One is that the two paths are widely separated and are traversed only once; the other is that the region of localization of the fringes can be made to coincide with the test object, so that an extended source of high intensity can be used. The experimental setup presenting the application of Mach-Zehnder interferometry to breakdown in liquids is shown in Figure 3.

In all the above methods (interferometry, Schlieren, and shadowgraphy), the image formation relies on refractive

index changes. However there are some important differences between these techniques.

(1) Interferometry has a larger number of optical elements. Since it is based on differential phase measurements, it is sensitive to alignment. Schlieren technique has fewer optical components and is less sensitive. Shadowgraphy, being the simplest configuration, is the least sensitive to factors like alignment, vibrations, and other extraneous effects.

(2) Interferograms are clear and useful in experiments with low density gradients. However the intensity contrast in Schlieren and shadowgraphy may not be large enough to provide a vivid picture. In high gradient experiments, both Schlieren and shadowgraphy yield clear and interpretable images. Interferograms are corrupted by refraction errors.

(3) In unsteady flow fields, Schlieren and shadowgraphy track temporal changes in temperature and concentration in the form of light intensity variations. These are less obvious in interferograms where information is localized at fringes.

(4) The number of fringes formed in water is large, since the sensitivity of refractive index to density is large in such media. Interferograms recorded in such experiments are affected by refraction errors. Schlieren and shadowgraphy have an advantage in this respect. However, interferograms can provide information about physical data of the experiment which cannot be obtained from Schlieren and shadowgraphy.

(5) In experiments with shockwave formation, interferography has an advantage since it can provide much sharper borders of the shockwave front.

(6) Shadowgraphy and Schlieren have the advantages of low cost and simplicity of apparatus and ease of real-time qualitative interpretation. However, Mach-Zehnder interferometry has the advantage of providing quantitative information.

4. The Structure of Optical Breakdown in Liquids

Most studies of the phenomena of optical breakdown in water refer to the dynamics of the radiation emitted from the breakdown region and only a few address the integral hydrodynamic picture of the process. Understanding the optical breakdown mechanism in liquids, formation of laser spark columns, and their time evolution are of considerable importance to a variety of tasks. These include biomedical applications, plasma-mediated eye and biological tissues surgery [43, 44], selective cell targeting with light-absorbing nanoparticles, chemical engineering, and generation of micro/nanoparticles. It is also relevant to numerous analytical applications based on laser plasma spectroscopy [45–48]. Laser-induced breakdown mechanism in air and in solids is well established [49–54]. The hydrodynamic characteristics of laser-induced breakdown in water, as well as in some other liquids, have also been studied [24, 50, 53–62]. In earlier studies [25, 55–57], the breakdown was analyzed at microsecond resolution, which was not sufficient for revealing the early stages of the breakdown mechanism. Better spatial and temporal resolution down to the ns range allowed a better insight into the breakdown phenomenon [63–65]; however, the discrete structure of the laser spark column was not observed. Microsperical shockwaves in liquids were investigated [24] and numerical simulations have also been carried out. Such simulations and experimental data on plasma dynamics [64, 66] and shockwave formation [28, 64, 67] explained the cavitation dynamics and bubbles arising in water after breakdown and lasting longer than 1 μs [65, 68]. It has been suggested that plasma formation in water is initiated by electrons generated by multiphoton absorption in the liquid itself or in persistent impurities [64, 69, 70].

In almost all published articles in the last few decades the laser spark column in water was considered as a continuous object. The discrete structure and dynamics of laser spark columns in water have been only recently revealed by applying shadowgraphy and Schlieren diagnostic techniques [71, 72]. These high temporal and spatial resolution techniques allowed, for the first time, determining the discrete structure of the breakdown in its early stages. The laser spark in water was interferometrically imaged at its earlier moments of time. The application of Mach-Zehnder interferometry provided both high spatial and temporal resolutions, as was needed for studying the discrete microscopic structures of a laser spark column.

The structure of the laser spark depends on the laser beam characteristics, on the liquid (including its contaminants), and on time. We shall first address the structure of the laser spark columns in water and their dependence upon the nature of persistent impurities. These microscopic solid particulates initiate the plasma formation. In principle, double distillated water (DDW) should not contain any particles. In practice, the distillation process is not free of contamination and any exposure to air contributes to considerable additional contamination. The actual particulate concentration in DDW slightly exposed to air is ca. $2 \cdot 10^4$ cm^{-3}. This concentration is at least two orders of magnitude lower than that usually found in tap water. Filtration of tap water through 0.45 μm pore-size filter reduces the particulate concentration to ca. $1 \cdot 10^5$ cm^{-3} and a 0.22 μm pore-size filter can further reduce the concentration to ca. $3 \cdot 10^4$ cm^{-3}. Therefore, tap water, DDW, and filtered water were all good media for investigating the breakdown threshold in the presence of impurities.

Time-resolved breakdown in tap water can be imaged using Schlieren technique and some representative results are shown in Figure 4. One can see that shortly (a few ns) after the laser pulse the laser spark column is filled with microplasma balls of tens of μm in size. The avalanche ionization is probably responsible for the observed luminous balls over the particulates [20]. In a few nanoseconds the particulates are evaporated and the thermal explosion of the vapors creates microbubbles, as the surrounding water is forced out. These microbubbles and the associated shockwaves evolve in time as shown in this figure. These images demonstrate the

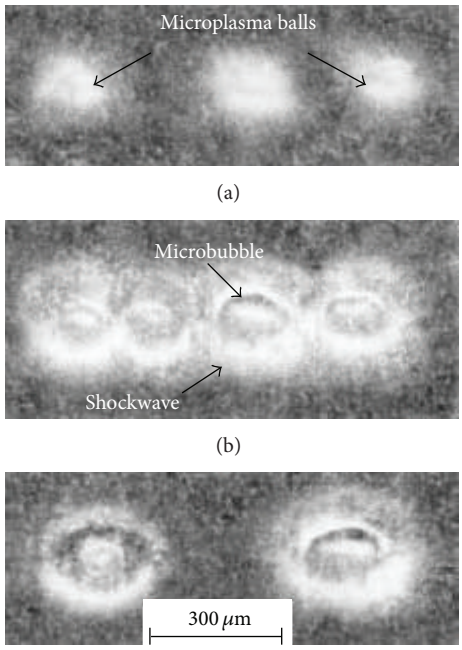

Figure 4: Examples of dark field Schlieren pictures of a part of the laser breakdown area in tap water. Laser pulse energy: 74 mJ. Time delay of the diagnostic light: (a) 1 ns, (b) 14 ns, and (c) 102 ns. Reprinted from [71], with permission from Elsevier.

capabilities of Schlieren technique to provide time-resolved images of breakdown events in water.

Similar temporal resolutions (in the low ns range) can also be achieved using Mach-Zehnder interferometry. It provides more detailed information on laser sparks in liquids, with spatial resolution of ≤10 μm. The shifts of the interference fringes and their sign allow calculating the local changes of the refraction index in the examined liquids. For example, a region compressed by a shockwave has positive refraction index change. This can be deduced from the corresponding sign of the fringe shifts. A region warmed by the laser radiation has negative refractive index change. Positive and negative changes of the refraction index lead to fringe shifts in opposite directions, perpendicular to the fringes.

The basic features of the breakdown in liquids are schematically presented in Figure 5. Numerous plasma events are formed in the vicinity of the focal point and along the laser beam. All of them together form the so-called laser spark column. It consists of microplasma balls, microbubbles, and spherical shockwaves of well-defined front (which were clearly presented in the Schlieren picture in Figure 4).

During the laser radiation time, a warmed channel is formed in the liquid along the laser beam. In some liquids, such as alcohols, this channel results in a cylindrical shockwave propagating apart from the laser beam. In water, a different kind of cylindrical shockwave evolves at longer times: the spherical shockwaves expand and interfere with each other. These interferences result in a cylindrical pattern, called interfering shockwave cylinder.

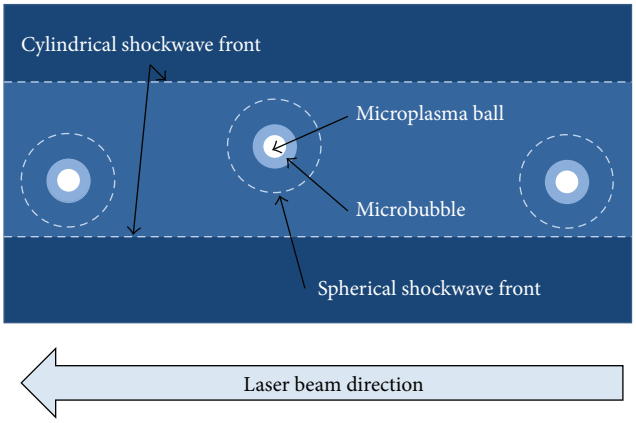

Figure 5: Schematic structure of a laser spark column. Reprinted from [72], with permission from Elsevier.

We shall now address the various time domains in the breakdown life. Clearly, the discrete structure of laser spark columns is formed during a few ns after the heating pulse. The laser spark evolution is conveniently divided into three major time intervals: the first stage (τ_d < 50 ns), the second time stage (50–200 ns), and the third stage (>200 ns). These are discussed in the following.

The first 50 ns of the spark generation is presented in Figure 6. At the end of the laser pulse (of ca. 5 ns) the spark column is full of luminous microplasma balls of ca. 100 μm diameter. They arise due to avalanche ionization in the vapors of ablated material and successive heating of the plasma due to the bremsstrahlung effect. The vapors move as a piston working on the surrounding liquid and generate a powerful microsperical shockwave in it. The microplasma balls last up to ~1 μs. Since the plasmas are generated at the surface of particles, the initial sizes and characteristics of the microplasma balls within the plasma column depend on the nature of the suspended particulates and on their concentration. It can be seen that the size of the microplasma balls monotonically increases in the first ca. 500 ns, in both water and alcohols [71].

In both tested liquids, the microsperical shockwaves are getting clearly visible in about 20 ns. However, while in water the size of the spherical shockwave fronts is remarkably larger than the size of microplasma balls, in ethanol the size of the spherical shockwaves only slightly exceeds that of the luminous microplasma balls. Also the speed of the shockwaves (visible as coaxial rings) is larger in water (measured at the same time). This can be attributed to the much lower compressibility of water ($4.4 \cdot 10^{-10}$ Pa^{-1}) compared to ethanol ($11.0 \cdot 10^{-10}$ Pa^{-1}) [73].

Note that no shockwaves are observed in butanol at time delay of 10.5 ns. At this early time the spherical shockwaves have been just formed and have not yet detached from the microplasma balls.

The concentration of the induced plasma balls depends on the tested liquid. It is of the orders of $60 \cdot 10^4$ cm^{-3} in water and $2 \cdot 10^4$ cm^{-3} in ethanol. These concentrations can be compared to the concentration of particles in these

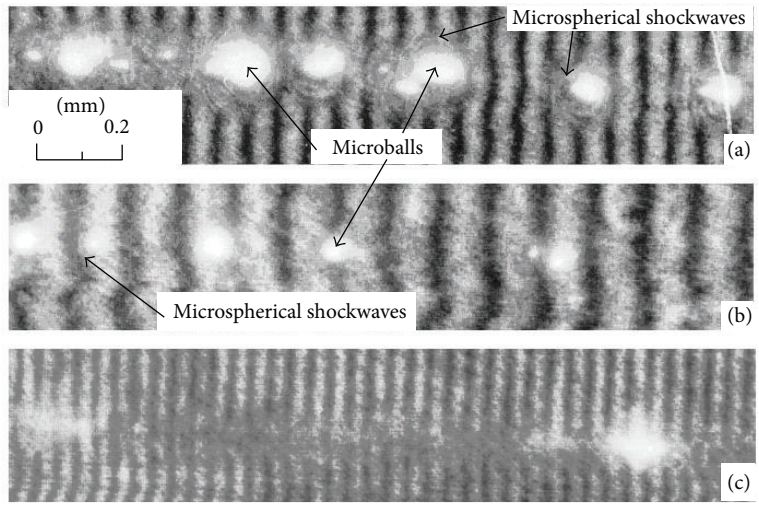

Figure 6: Fragments of interferograms of laser spark columns at the first time stage: $\tau_d < 50$ ns: (a) in water, time delay $\tau_d = 17$ ns; (b) in ethanol, $\tau_d = 22$ ns; (c) in butanol, $\tau_d = 10.5$ ns. The laser pulse energy was 70 mJ. The laser beam was focused from right to left. The focal spot coincides with the picture's left margin. Reprinted from [72], with permission from Elsevier.

liquids. In tap water only about 50% of the particles ignited breakdown processes, while in ethanol almost all particles were associated with plasma events. The differences might be attributed to the differences in size distribution and in the chemical nature of the suspended particulates. Nevertheless, the large percentage of particles involved in the breakdown mechanism supports the model of the discrete nature of plasma generation in liquids.

The second time rage in the spark's life starts at 50 ns and lasts till 200 ns. It is characterized by larger microbubble sizes and spherical shockwaves. This process is illustrated in Figure 7, where both the large microbubbles and the associated spherical shockwaves are clearly imaged. The microbubble sizes are larger than those of the microplasma balls.

At this time domain, the characteristic size of the spherical shockwaves is comparable to the average distance between suspended particles. Therefore, an interfering shockwave cylinder is formed, as a result of overlapping neighboring spherical shockwaves. This is manifested in a mixture of interferometric fringes of cylindrical symmetry. Note that, in the past, this cylindrical shockwave was considered as a continuous object, since the old experimental setups were not able to resolve the discrete structure of the laser spark column [50, 59–62]. It is now clear that when the spherical shockwaves emerge in a cylindrical pattern (50–90 ns), it is still a shockwave (Mach number >1). Only at later times does it become a strong acoustic wave.

As the spark evolves beyond 200 ns, the size of the microbubbles becomes remarkably larger than the diameter of the microplasma balls. The evolution of microbubbles and spherical shockwaves in this range is shown in Figure 7. Also the interfering shockwave cylinder becomes a cylindrical acoustic wave, which is clearly observed and its radius is much increased.

It is at this stage that the plasmas change from discrete nature to continuous one. The cylindrical shockwaves are merged into spherical shockwaves. This happens when the numerous microsperical shockwaves expand and combine into a single cylindrical shockwave. The transformation that the spark undergoes from discrete nature in the very beginning to a continuous event at longer times is a recent concept. Cylindrical shockwaves were well recognized [25, 74]; however, the experimental setups used in the past did not allow for observing this transition. The old measurements were carried out either at too long times (of ca. 6 μs), when only the continuous spark could be observed, or at short times but using experimental setups that did not allow for observation of the discrete events. Therefore only the new interferometric measurements were able to reveal the mechanism of the formation of the cylindrical shockwaves.

The above described spark generation mechanism is valid under most experimental conditions, where the laser focusing is moderate and the liquid contains a reasonable concentration of particulates. This might not always be the case. Under very sharp focusing conditions and at very low particulate concentrations, the mechanism might be different. Under such sharp focusing conditions, spherical shockwaves are expected and not cylindrical. If the particulate concentration is very small such that not even a single particle is present in the focal volume, the mechanism of the breakdown might be different. This was probably the case when much shorter plasma luminescence lifetimes were observed [66, 75]. However, it was found that, in most commercially available liquids of analytical grade, there are a few particles present in the focal volume of a singlet of $f = 50$–100 mm, and at least 1-2 breakdown events can be observed.

5. Breakdown Dynamics in Suspensions

5.1. Temporal Resolution. Interferometric imaging methods allow for detailed investigation of the time dependent evolution of the laser-induced microbubbles and the associated

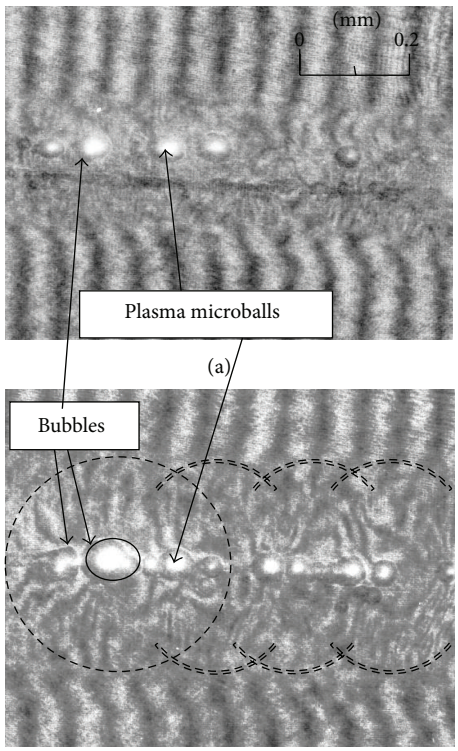

Figure 7: Fragments of interferograms of laser spark columns in ethanol. The laser pulse energy is 70 mJ. The laser beam is focused from right to left. The focal spot coincides with the picture's left margin. (a) Delay of 152 ns (second time range); (b) delay of 333 ns (third time range). Dotted circles mark spherical shockwave fronts. Reprinted from [72], with permission from Elsevier.

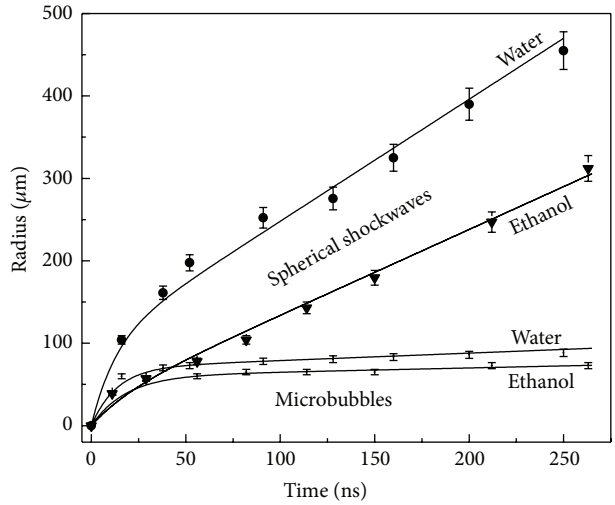

Figure 8: Experimental dependence of microbubbles and associated spherical shockwave radii in water and in ethanol as a function of time; energy of the laser pulse was 65 mJ. Reprinted from [72], with permission from Elsevier.

shockwaves. For example, the radii of the microbubbles and of the surrounding spherical shockwaves in water and ethanol as a function of time are presented in Figure 8. The results support the following interpretation of the breakdown dynamics. First, the suspended particulates in the irradiated liquid absorb the laser pulse. The surfaces of these inclusion particles begin to evaporate and at the same time the expanding motion of the vapors is strongly restricted by the surrounding water. This leads to high pressures, which support the ionization avalanche. Multiphoton absorption and ionization cause the appearance of the first electrons [76–78]. The expanding vapors act as a spherical piston, which effectively compresses a layer of liquid and generates a spherical shockwave in this medium. This shockwave starts its expansion with supersonic velocity together with the microbubble walls. After a certain time the shockwave outdistances the microbubble wall, leaving it behind.

This qualitative interpretation is also supported by a quantitative description and modeling of the process: the expansion of the plasma is often considered as a thermal explosion, approximated by the known dynamics of a point blast [76, 79]. This model describes the situation in which a large amount of energy is liberated in a small volume during a short time interval:

$$R_c = \left(\frac{E_i}{\rho}\right)^{1/5} \tau^{2/5}, \quad (1)$$

where R_c is the radius of the microbubble, E_i is the laser energy absorbed by the particle during the laser pulse, ρ is water density, and τ is time.

The energy E_i is proportional to the energy of the laser beam E_{lp} and depends on d_i, the size of the particle, and d_F, the diameter of a focal spot:

$$E_i \approx \left(\frac{d_i}{d_F}\right)^2 E_{lp}. \quad (2)$$

Equations (1) and (2) provide

$$R_c \approx \left(\frac{d_i}{d_F}\right)^{2/5} \left(\frac{E_{lp}}{\rho}\right)^{1/5} \tau^{2/5}. \quad (3)$$

In this model the microbubble size depends on the laser radiation and on the size of the particle which has induced the plasma. Evaluating dR_c/dt shows that the microbubbles expand at supersonic velocity only during the laser radiation time. Afterwards, the expansion rapidly slows down and after ca. 20 ns they start moving with subsonic velocities. This is clearly confirmed in Figure 8: up to ca. 10 ns the microbubble and the shockwave are moving together at supersonic speeds. After that the shockwave outdistances the microbubble.

The Mach numbers of the spherical shockwave fronts are shown in Figure 9 for two liquids. The graphs indicate that the expanding velocities of the spherical shockwaves and of the microbubbles in water are remarkably higher than in ethanol [73]. This is attributed to the higher compressibility of ethanol and to the lower speed of sound in this liquid (1.16 km/s in

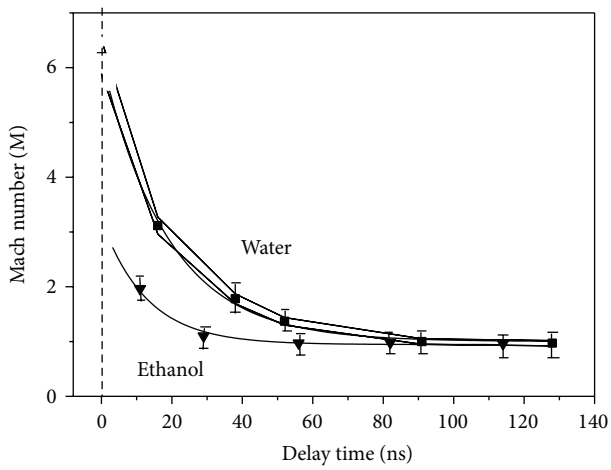

Figure 9: Mach number of spherical shockwaves as a function of time. Reprinted from [72], with permission from Elsevier.

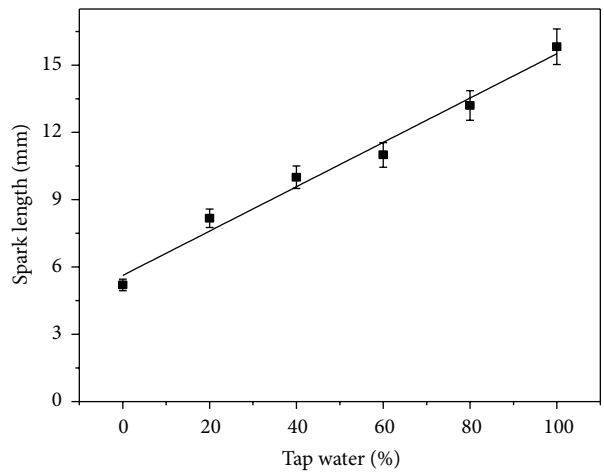

Figure 10: Experimental dependence of laser spark length on concentration of tap water in mixtures of tap/pure water at fixed laser pulse energy of 70 mJ.

ethanol and 1.46 km/s in water). The lower compressibility of water may also lead to higher pressures at the shockwave front.

Similar investigations were carried out for laser plasmas in continuous media [64]. Comparison to these data indicates that the shockwaves around a particle are much more intensive than those from a plasma spark column.

5.2. Microbubble Radius as a Function of Energy. According to (1) the microbubble radius depends on the energy of the laser pulse absorbed by the particle. This model of plasma generation in water suspensions cannot be directly confirmed, since in this medium the laser pulse simultaneously generates numerous microbubbles. However, the statistical validity of this model can still be tested using shadowgraphic measurements obtained at the same delay time and at different laser energies. The results have shown that at each energy there is a distribution of microbubble radii. Higher pulse energy generates a larger concentration of microbubbles in the focal volume and these are of larger average radii.

Using the relation $R_c \sim E_p^{1/5}$ and summing over a measured set of microbubbles provide

$$\frac{E_N}{E_M} = \frac{\sum_{n=1}^{N} \left(R_{c,n}\right)^5}{\sum_{m=1}^{M} \left(R_{c,m}\right)^5}, \tag{4}$$

where N and M are the numbers of microbubbles of radii $R_{c,n}$ and $R_{c,m}$, formed when the absorbed energies are E_N and E_M. This measured ratio was ≈2.4. This result correlated well with the ratio of the actual absorbed energies E_N/E_M, which was ≈2.4.

5.3. Plasma Column Length. A significant difference between the plasma generated in liquids and that generated in air is its structure: in air, a single plasma spot is observed, while in liquids numerous tiny plasma spots are generated. These appear in a column extending in the axis direction on both sides of the focal point. The actual length of this column is a function of laser pulse energy.

Theoretical investigations [28, 31] have indicated that the length of the plasma column, z, increases with the laser irradiance according to

$$z = z_R \left(\beta - 1\right)^{1/2}, \tag{5}$$

where β is the ratio of the peak power of the laser pulse to the breakdown threshold and z_R is Rayleigh's length. Quite interesting, the experimental z values do not quantitatively agree with those calculated in this model. The experimentally obtained results remarkably exceeded the values calculated using (5).

In water suspensions, the length of the laser spark column depends on the concentration of particles and on their size distribution and it increases with the particulate concentration. This effect was demonstrated by measuring the spark column length in pure water (DDW), in tap water, and in a series of mixtures of pure and tap water. The particulate concentration was $2.5{\cdot}10^4$ cm^{-3} in the DDW and $1.2{\cdot}10^6$ cm^{-3} in the tap water. The results are shown in Figure 10, for fixed laser pulse energy of 70 mJ.

5.4. Breakdown Threshold in Suspensions. Generation of plasma requires laser pulse energies over a specific threshold. Usually, this threshold is defined statistically, since plasma generation close to the threshold has a specific probability [78]. This definition of the threshold is problematic, since it requires numerous measurements and statistical evaluation of the results. A new definition of the breakdown threshold has been recently suggested [71].

Experimental results showed that the plasma column length depends on the amount of energy absorbed by the plasma, as presented in Figure 11. The intercept of the corresponding regression line with the x-axis indicates an energy value which generates a plasma column of zero length. In tap water this value is 13 mJ, which can be considered as

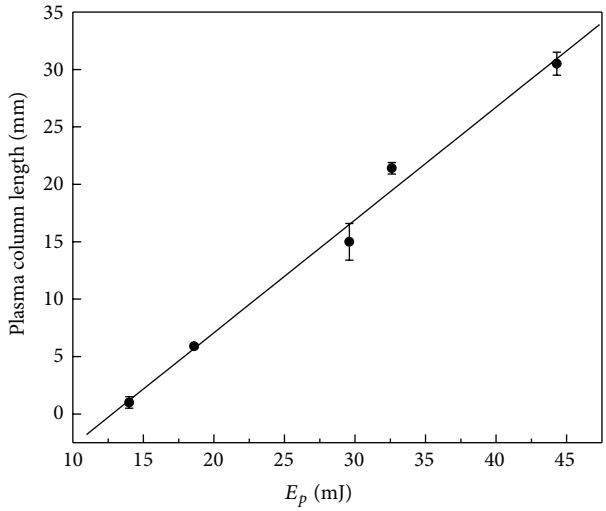

Figure 11: Length of the plasma column as a function of the absorbed energy.

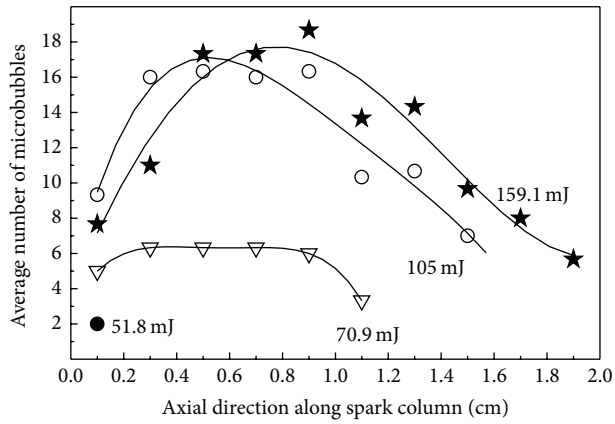

Figure 12: Average number of microbubbles as a function of location along the spark column for various laser pulse energies. Each point represents an interval of 2 mm. Laser beam direction was from right to left. Reprinted from [72], with permission from Elsevier.

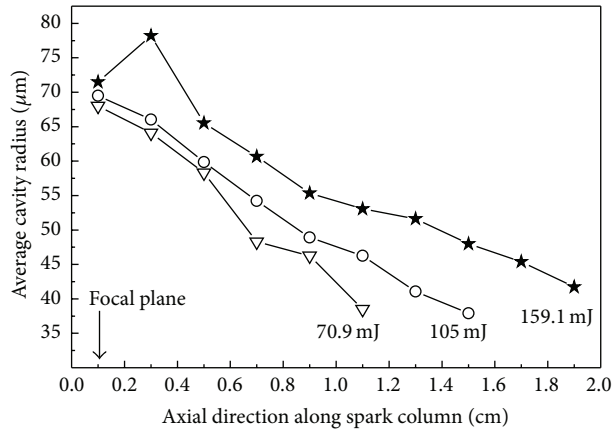

Figure 13: Average microbubble radius as a function of location along the spark column, for various laser pulse energies. Each point represents an interval of 2 mm. Laser beam direction was from right to left. Reprinted from [71], with permission from Elsevier.

the breakdown threshold. This definition of the threshold is readily obtained and does not depend upon statistical assumptions.

Measurements of the experimental breakdown threshold in pure water (DDW) resulted in a value of 15.8 mJ. The threshold in tap water was 5.0 mJ [71]. The breakdown threshold defined by extrapolation to zero plasma column length is higher by the factor of ~3 in pure water. Other results, using a different breakdown threshold definition, indicated a factor of 5 for ns laser pulses [80].

5.5. The Number of Microbubbles and Their Size along the Laser Spark Column. The number of microbubbles and their size along the laser spark column can also be analyzed from the plasma shadowgraphs. The average number of microbubbles as a function of the location along the laser spark column is shown in Figure 12. In all studied cases the microbubble concentration had a maximum, which was found ahead of the optical focus. The absolute number of microbubbles increased with the laser energy. However, it is interesting that the location of the maximal microbubbles concentration moved towards the laser source, as the energy increases. This was attributed to the shielding of the laser light by the plasma and to effects related to modifications in the matrix optical properties at high laser powers.

While the microbubbles concentration possesses a maximum, their average radius monotonically increases along the laser irradiation axis and reaches a maximum value close to the optical focal plane (Figure 13). The average microbubble radius in each interval along the plasma column strongly depends on the laser pulse energy.

5.6. Spatial Distribution of the Absorbed Laser Energy along the Spark Column. Elemental chemical analysis based on plasma emission depends on absorption of laser radiation. Integrated spectral data collect considerable noise, mainly from the peripheral locations where only little laser absorption takes place. Therefore, optimization of spectral measurements requires information on the spatial distribution of the absorbed laser energy along the spark column.

The measurement of microbubble sizes and concentrations can be used as a diagnostic tool for characterizing the spatial distribution of the absorbed laser energy along the laser spark column. This requires the assumption that the absorbed energy is proportional to the sum of the values R_c^5 along the laser spark. The results (shown in Figure 14) indicate that the maximal absorption of the laser beam takes place close to the focal point. As expected, at lower energies the absorbed energy monotonically decreases in the axial direction. However, at the highest energy (of 160 mJ) a local maximum was observed just before the focal point. This was explained in terms of the plasma shielding effect. Another possible explanation was that at high energies the focus moves

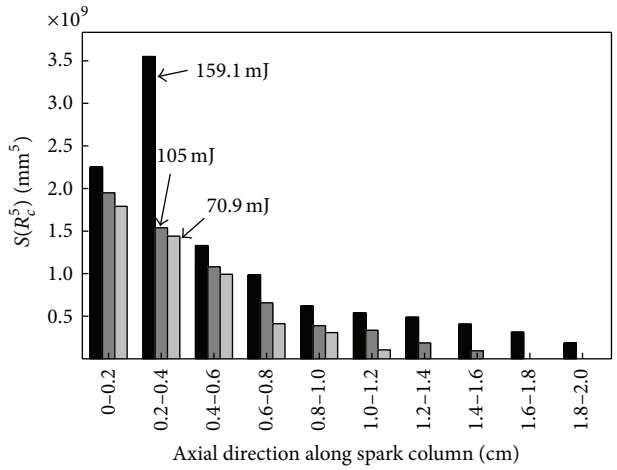

Figure 14: Axial distribution of the absorbed energy along the laser spark column for different laser pulse energies. The laser beam direction was from right to left. Reprinted from [71], with permission from Elsevier.

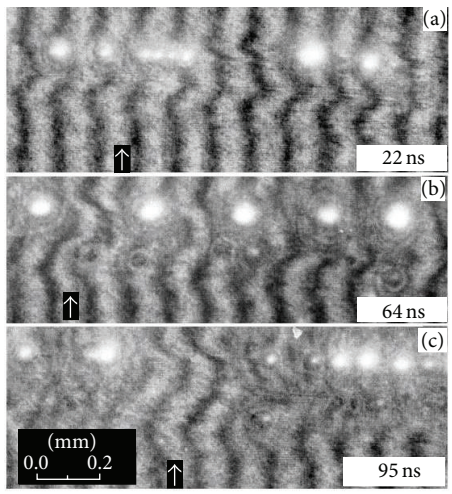

Figure 15: Fragments of interferograms measured at different time delays, illustrating the dynamics of a warmed channel in ethanol. The output of the laser pulse was 65 mJ. The radiation goes from right to left. The arrows indicate the planes where the radial distributions of the refraction index were calculated. Reprinted from [71], with permission from Elsevier.

towards the heating laser source due to nonlinear effects such as self-focusing.

5.7. Warmed Channels in Liquid Suspensions. The laser radiation might form warmed channels in liquid suspensions. It has to be taken into account especially in spectral measurements performed at high repetition rates. Interference imaging allows for measurement of this effect in the focal volume region.

The temperature change, ΔT, was estimated using the interference measurements. The change in the refractive index was approximated using the following expression: $\Delta n = \Delta k\lambda/dc$, where Δk is the experimentally measured fringe shift in the warmed region, λ is the wavelength of the diagnostic radiation, and dc is the diameter of the warmed region. This way, the temperature change was estimated as

$$\Delta T = \frac{\Delta n}{(\partial n/\partial T)_\rho}. \quad (6)$$

For water, the constant $(\partial n/\partial T)_\rho = -0.8 \cdot 10^{-4}$ [81]. Therefore, the corresponding temperature change in water is $\Delta T \approx 50$ K. This value was in agreement with the result obtained from conservation of energy consideration. It was found that the warmed channels in water last more than 1 μs and then they are deactivated by the process of thermal conductivity.

A different mechanism was observed in alcohols. In this case the warmed channels generate cylindrical shockwaves, expanding in radial direction. The dynamics of such cylindrical shockwaves in alcohols are interesting and are described in the following.

5.8. Dynamics of Cylindrical Shockwaves in the Alcohols. The dynamics of the cylindrical shockwaves generated in alcohols were obtained from interferograms of the warmed regions. Examples of the interferograms obtained from ethanol suspensions and the associated cylindrical shockwaves at several

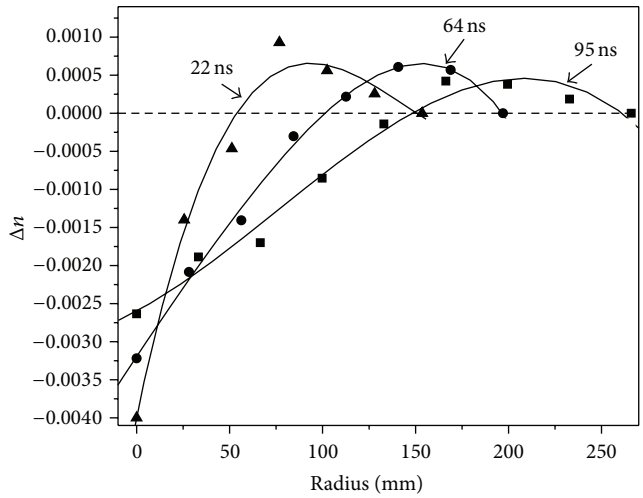

Figure 16: The calculated radial distribution of the refraction index of ethanol in the warmed region at three time delays. The data characterize the cylindrical shockwaves. Reprinted from [72], with permission from Elsevier.

delay times are shown in Figure 15. Such data were used for calculating the corresponding changes in the refractive index in the warmed channel and in the associated cylindrical shockwave.

The radial distribution of the refraction index change in ethanol is presented in Figure 16. In general, warming of the liquid is associated with reducing the index of refraction, while compression in the shockwave increases the index of refraction. The maximum negative change of the refractive index is on the axis of the heating beam ($r = 0$), where the temperature achieves a maximal value. The maxima in this figure indicate the locations of the higher compression,

namely, the shockwave fronts. As time evolves, the maxima are found at larger radii. The results also indicate that the quantity of the thermal energy absorbed in the focal volume is sufficient for generating the cylindrical shockwave. It moves in radial direction with the speed of ~1.5 km s^{-1}. This way, the actual temperature change at any time delay and location could also be estimated. For example, the temperature change in ethanol, at 22 ns and at $r = 0$, was $\Delta T \sim 10^{\circ}$K.

No cylindrical shockwaves were observed in water suspensions. Estimations have shown that the energy absorbed in water is dissipated by thermal conductivity. Full explanation of this difference between water and alcohols is not yet understood. A possible explanation was suggested, based on the differences in the coefficient of volumetric thermal expansion of these liquids.

The cylindrical shockwaves were observed in many alcohols. The dynamics are, in principle, very similar: starting their motion with supersonic speeds the cylindrical shockwaves quickly decelerate and expand asymptotically approaching the speed of sound.

6. Analytical Applications of Laser Breakdown in Water Suspensions

6.1. LIBS Method. Laser-induced breakdown spectroscopy (LIBS) is a multielemental analytical method based on time-resolved measurement of atomic emission lines from laser plasma generated at a sample surface or inside. The most appealing quality of LIBS is the potential of remote and in situ applications. LIBS offers the ability to transfer the laser energy through an optical fiber to generate plasma and transport the resulting emission back through the fiber to a remote spectrometer, while keeping the sample free from contamination and the analyst isolated from potentially harmful environments.

The advantages of LIBS for direct spectrochemical analysis include the following: (a) no or little sample preparation needed; (b) versatile sampling of all media; (c) very small amount of sample vaporized; (d) ability to analyze extremely hard materials that can hardly be digested or dissolved, such as ceramics and superconductors; (e) local analysis in microregions offering a spatial resolving power of about 1–l00 μm; (f) possibility of simultaneous multielement analysis.

Good analytical performance requires high signal to noise ratio. At the very beginning of the plasma formation a continuum light emission takes place; this tends to overshadow the emission lines from the excited species in the plasma. Thus, the LIBS spectral acquisition has to be delayed until the plasma cools down. This may improve the signal to background ratio. The delay time (t_d) is the time between the laser pulse and the starting of the spectral acquisition. The gate width (t_w) is the time period over which the plasma light is collected [6]. By using a time-resolved detection system to control t_d and t_w, the intense initial continuum emission at the early stage of the plasma formation can be gated off, and the signal to noise ratio can be improved dramatically. It was found that gate width longer than 50 μs was unnecessary because most of the analytical emission lines had completely decayed [82].

LIBS performance is often affected by environmental factors, instrumental parameters, the chemical and physical properties of the sample, and the homogeneity and the ambient states of the sample. Many instrumental parameters have been optimized, including air humidity, temperature and pressure, laser pulse energy [83, 84], pulse duration [85], pulse repetition rate [86], laser wavelength [87], delay time and gate width [58–89], and the number of laser shots [90].

The LIBS spectra contain large and complex information about the elemental composition of the sample, which can be used for qualitative as well as quantitative analysis of many elements. In a matter of microseconds, tens of thousands of data points can be collected. Therefore, the use of a suitable chemometric data analysis method to efficiently and accurately analyze the complex LIBS spectra is of considerable importance. Several relevant algorithms have been developed [91–93]. In most applications, LIBS spectra are analyzed using univariate approach (based on single emission lines), which causes the loss of useful information [94, 95]. However, also multivariate analysis methods have been applied to LIBS [96–100]. The results indicated that using several emission lines in combination provides improved performance [97, 101].

6.2. LIBS of Water Suspensions. Direct application of LIBS to analysis of various materials in bulk liquids results in very low spectral intensities [102, 103]. This might be surprising, since LIBS works well for aerosols in air [11, 104–106] or on solid particulate samples [107–113]. Even analysis of individual aerosol particles in air was successfully accomplished [106]. The main difference in water is that this medium, in contrast to air, suppresses the plasma expansion, which results in reduced sensitivities. The plasma emission in water has a very short lifetime and consists of a superposition of the elemental lines over a wide and intense continuum emission.

In order to overcome these problems, several alternative methods were developed. For example, a coaxial nozzle was used in order to enhance the spectral intensities obtained from colloidal iron. The nozzle generated a constant flow and the stream of water was irradiated by a laser pulse. This method resulted in much higher LIBS intensities than in liquid bulk and allowed for the determination of colloidal iron in the low ppm concentration range. Another approach was the collection of the suspended particles on a filter for subsequent LIBS analysis. This way, analysis of biological materials such as pollen, bacteria, molds, fungi, and viruses in water could be carried out [114, 115]. Similarly, boron, uranium, and thorium [116, 117] were also analyzed in water and results in the low ppm range were obtained. Filter assisted LIBS analysis was also developed for analysis of single biological microparticles such as pollens [118]. The measurements showed that bioaerosols could be distinguished from other common aerosols, for example, dust. Also *E. coli* bacteria could be identified on paper filters using LIBS [119]. Samples were prepared by aspirating a solution of bacteria on a filter paper and drying for an hour. The results showed that the samples could be characterized by their profile of spectral intensity and varieties of trace mineral elements. These trace elements are divalent cations, which maintain the cohesion

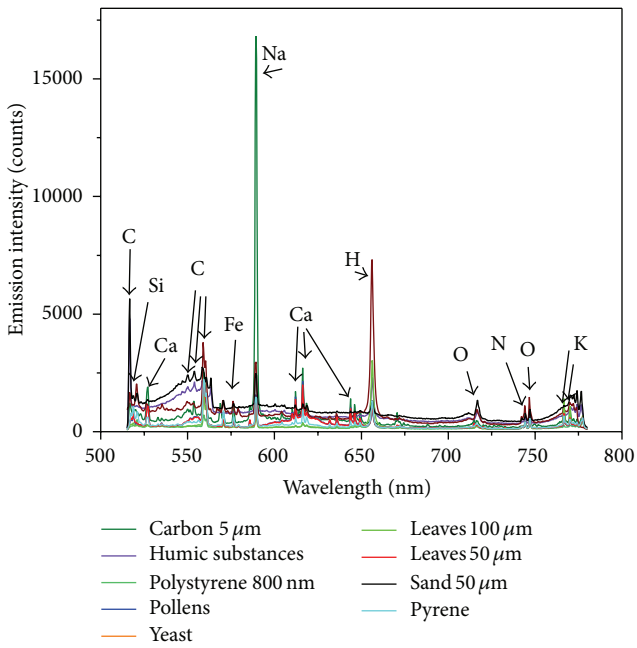

Figure 17: LIBS raw spectra of a set of suspension materials. The gate delay was 2 μs and gate width was 10 μs. The laser pulse energy was 230 mJ.

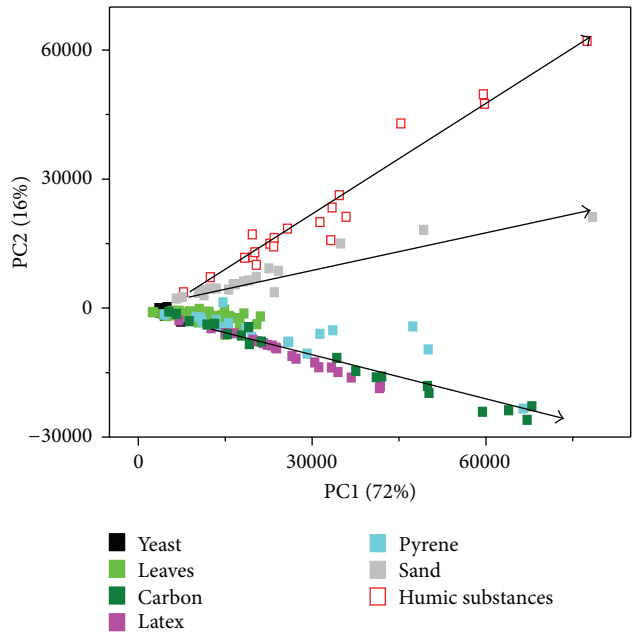

Figure 18: Principal component analysis (PCA) score plot of raw LIBS spectra.

of proteins in the outer bacterial membrane. It comes out that bacteria may be identified based on these trace mineral elements.

The main problem in LIBS analysis of suspended materials is explained by the following example. Figure 17 shows full LIBS spectra of a series of suspension materials. These include organic, inorganic, and biological particles, which represent particles naturally persistent in water. The tested materials were as follows:

(a) organic matter of biological origin: leaves (50 μm) and pollens (*Acacia baileyana*);

(b) organic matter of nonbiological origin: carbon (5 μm), pyrene, polystyrene (800 nm), and humic compounds;

(c) biological matter: yeast (*S. cerevisiae*, representing eukaryotic microorganisms);

(d) inorganic matter: sand (50–100 μm).

The LIBS spectra of these materials contain multiple emission lines of many elements. Many of them contain similar elemental constituents: N, Na, K, C, Ca, Si, O, and H. Inspection of these spectra shows that simple analysis is not sufficient for distinction between the various materials. The conclusion is that LIBS analysis of suspended materials requires a statistical approach. Therefore, multivariate analysis was applied to these spectra, as described in the following.

6.3. Application of Multivariate Analysis to LIBS Spectra. Multivariate analysis (MVA) is an excellent tool for summarizing data of a large number of variables. Essentially MVA defines new variables that capture most of the variability associated with the collected data. Principal component analysis (PCA) is a basic MVA method that helps in understanding the common variations within a set of variables.

The simplest PCA approach to LIBS data includes its application to the raw spectra. A scores plot model was constructed, based on four components. This model clustered materials of similar composition, as can be seen in Figure 18. Each point represents a single laser shot. The first two principal components, PC1 and PC2, accounted for 72% and 16% of the spectral variability, respectively, while the remaining variability was described by higher PCs. These results confirmed that most of the sample set could be classified by this model.

Figure 18 shows three vectors that include all organic materials of nonbiological origin (pyrene, carbon, and polystyrene), sand, and humic substances. Organic materials of biological origin (leaves and yeast) were concentrated in one location on the plot. These materials have similar elemental composition of atoms such as N, Na, K, C, Ca, O, and H. Organic materials of nonbiological source have a high concentration of carbon and combined into one vector on the PCA score plot. Sand differs from the other materials because of its high Si concentration and thus it formed its own vector. Humic substances also differ from the other materials in their basic composition. This model allowed for easy detection of these particles in water.

Due to laser power fluctuations and due to the particulate nature of the suspended materials, LIBS spectra suffer from instabilities. Therefore, analysis based on the raw spectra might not be optimal for detection of particles. Many articles suggested utilizing peak intensity ratios in LIBS analysis [120–123]. For example, classification of explosive-containing

residues was successfully achieved using MVA based on the emission intensity ratios of O, H, C, Ca, and N lines. It was found that most explosives have higher O and N content relative to C and N. Thus, the atomic emission ratios could differentiate explosive organics from nonexplosive organics. Other ratios were useful in separating inorganic and organic samples. These findings indicate that identifying the correct peak ratios can improve the classification of suspended materials.

Concerning the above suspended materials, good results were obtained using PCA analysis of the discrete peak intensity ratios of C/H, Na/K, and Na/Ca. The thus obtained score plots are shown in Figure 19. The model was based on four components, where each point represented a single laser shot. This model grouped materials of similar composition. The first two principal components, PC1 and PC2, accounted for 77% and 17% of the spectral variability, respectively (94% together). These results indicated that the model based on these particular peak ratios performed better than the one based on the raw spectra. The model clearly identified four groups of materials: biological matter, humic substances, inorganic matter, and organic matter of biological and non-biological origin. As before, sand was well separated from the other materials on the score plot. This was attributed to the fact that this material has higher K and Na content relative to C, H, and Ca.

A separate group of all organic materials was expected, since they have a high concentration of carbon and their C/H peak intensity ratios are similar. However, the results showed that yeast was well separated from other materials. While all cells contain the same elements, the ratios differ between eukaryotic cells, which do not have a rigid cell wall, and plant cells, which have chloroplasts and vacuoles [124–126]. Hence, the C/H ratio of yeast differs from that of leaves. Therefore, this model was useful for separating particles of plant cells from eukaryotic cells, which are more harmful to humans. Actually, the combination of both models provided a very useful tool for analysis of suspended materials.

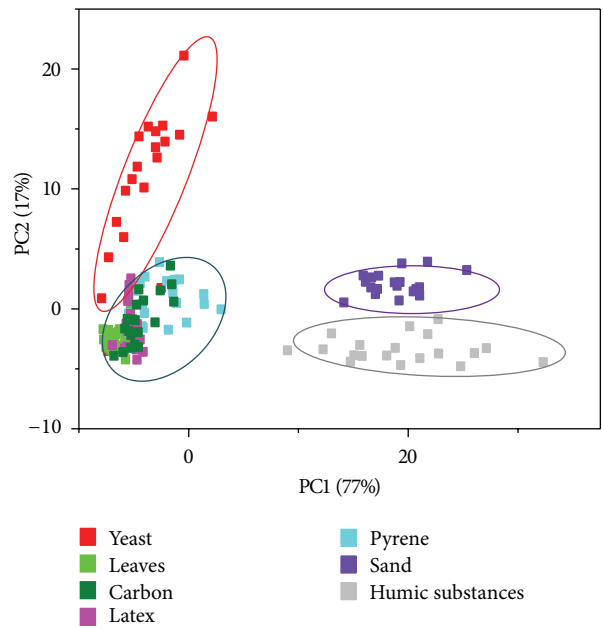

Figure 19: Principal component analysis (PCA) score plot of element peak ratios C/H, Na/K, and Na/Ca.

6.4. Application of Optical Breakdown in Liquids to Generation of Suspended Nanoparticles. Optical breakdown in liquids attracts much attention as a new technique of material processing [127]. In particular, generation of suspended nanoparticles is of considerable interest [128]. For example, the unique properties of gold and silver nanoparticles make them attractive in nanophotonics [129] and in biological labeling and sensing [130, 131]. Metallic nanostructures can be utilized in the development of sensors for volatile organic compounds (VOCs) and biomolecules.

Interferometric methods have the potential to elucidate the dynamics of the generation of suspended nanoparticles. The dynamic information can be used for optimizing the ablation process and for controlling the size and shape of the particles, as well as improving the yield.

6.4.1. Visualization of Suspended Nanoparticles Generation in Water. Visualization was carried out using time-resolved Mach-Zehnder interferometry, as previously described. The visualized process was initiated by irradiation of metal targets in double distilled water by a Nd:YAG laser (λ = 1064 nm, 6 ns). The laser was focused by singlets of different focal lengths.

The time-resolved interferograms obtained from irradiation of silver and gold targets are shown in Figures 20 and 21. These figures illustrate the different stages of the expansion dynamics of the high temperature plasma generated on gold and silver targets. The expanding plasma is associated with a strong shockwave in the surrounding liquid under the conditions of the well-developed vaporization. The surface plasma expands half-spherically and accelerates a layer of the surrounding liquid out of the target. In the early stages of plasma expansion, the associated shockwaves move in the water at supersonic velocities in opposite direction from the metal target. It seems that in these cases the dynamics can be approximated by the model of point explosion, with expansion into half-sphere.

At time delays of $\tau_d \leq 40$ ns the shockwave front propagates together with the plasma and moves with supersonic velocity. At longer delays, the front continues its motion with supersonic velocities and outdistances the contact boundary between the plasma and water. After this, the plasma rapidly decelerates its motion. Approximately this moment of time is illustrated by the interferograms in Figures 20(b) and 21(b). The detached spherical shockwave rapidly diminishes its speed and moves at moderate supersonic speeds in opposite direction from the target. For time delays longer than ~80 ns the shockwave asymptotically moves at the sonic speed in water (ca. 1.46 km sec^{-1}).

Clear differences are observed between gold and silver targets. In silver, the front of the shockwave is much wider

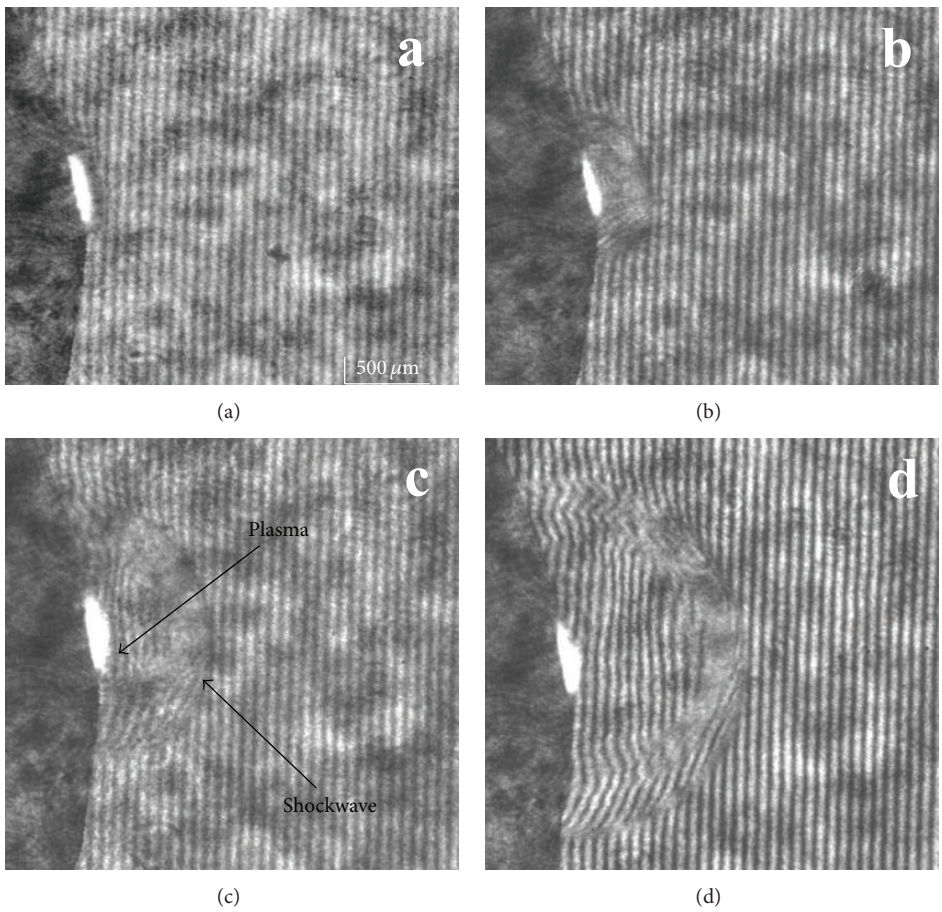

Figure 20: Interferograms measured at several time delays after the laser pulse: (a) 23 ns, (b) 163 ns, (c) 380 ns, and (d) 614 ns. The target was gold surface under water. The laser was focused using a lens of $f = 77$ mm and the power was 75 mJ (at target).

than in gold, which might indicate removal of more material from the bulk.

The time-resolved interferograms allow for estimating the shockwave radius as a function of time. This information can be converted (under certain reasonable assumptions) to expansion velocity as a function of time. The results are shown in Figure 22. Clearly, at the very beginning of the shockwave expansion, the velocities are higher for gold targets than for silver. After ca. 8 ns the order is reversed and at long times both shockwaves attenuate and reach the asymptotic $M = 1$ velocity.

6.4.2. Effect of Surface Energy Density on Particle Generation. The energy density at a gold surface target was varied by changing its distance from the focusing lens (of $f = 77$ mm). The laser pulse energy on the target was unchanged (75 mJ). The absorption spectra of thus generated water suspensions were measured. These spectra were measured since the absorption spectra of nanoparticles depend on their size and shape [80, 132–134]. The results are shown in Figure 23.

The results indicated that surface energy density plays an important role. The highest absorbance was observed at the highest surface energy density, which means that this parameter directly affects the particle generation yield. Moreover, the wavelength of maximum absorbance of gold nanoparticles in suspension indicates their morphology. In this particular case, the maximum absorbance peak was detected at 528 nm, which indicates that the mean size of the nanoparticles was ~35 nm. The wavelength of maximum absorbance is not affected by the surface energy density, which means that this parameter cannot modify the mean size of the nanoparticles.

6.4.3. Effect of Laser Pulse Duration on Particle Generation. The laser pulse-width controls the temporal distribution of the energy on the solid surface; thus, it can influence the particles production [134]. Evaluation of this effect was examined by using two different pulse lengths (at constant total pulse energy and under the same geometrical conditions). The short pulses were of 6 ns and the long pulses were on 120 μs. The absorption spectra of the suspensions obtained under these conditions were measured. The results for gold target are shown in Figure 24.

The first observation was that in both cases the wavelength of maximum absorbance is the same (528 nm). Therefore, the conclusion was that the mean size of the particles is not affected by the pulse duration (ca. 35 nm in both cases). However, the production yield was much different.

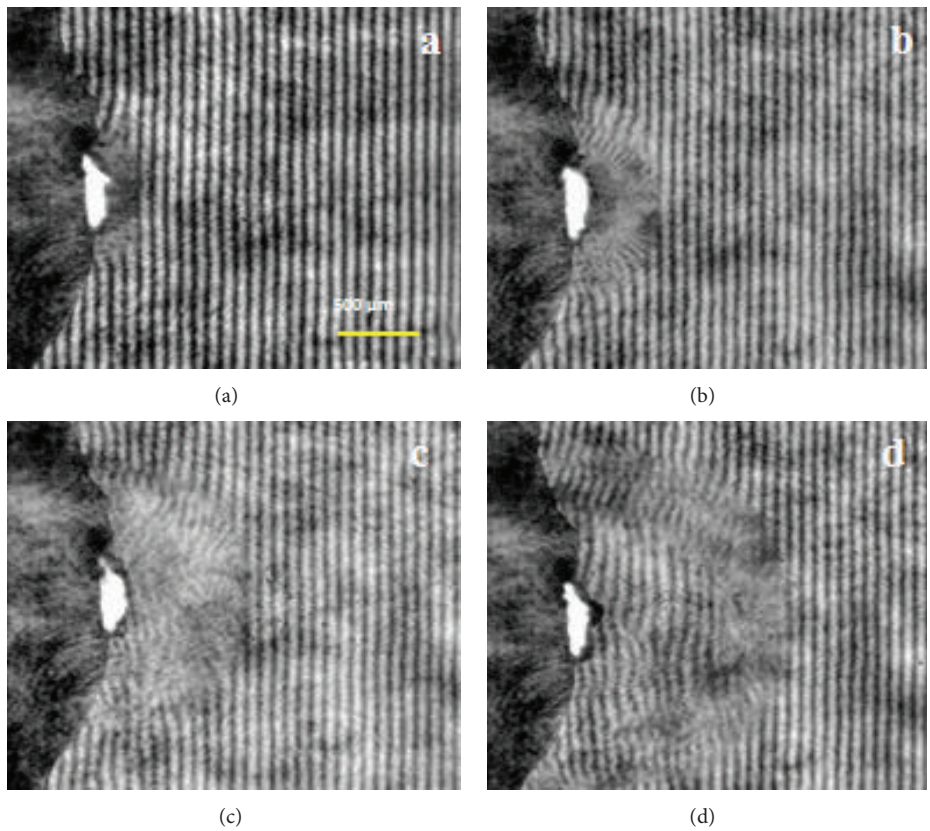

FIGURE 21: Interferograms measured at several time delays after the laser pulse: (a) 25 ns, (b) 173 ns, (c) 352 ns, and (d) 600 ns. The target was silver surface under water. The laser was focused using a lens of f = 77 mm and the power was 75 mJ (at target).

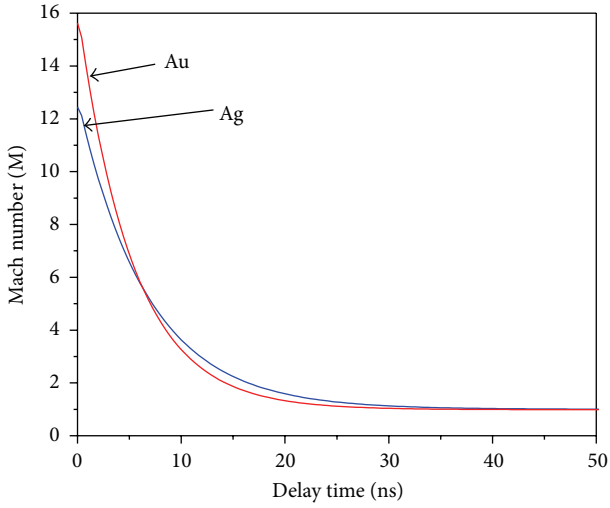

FIGURE 22: Shockwaves Mach numbers in gold and silver suspensions as a function of time; laser energy on target was 75 mJ, lens f = 77 mm.

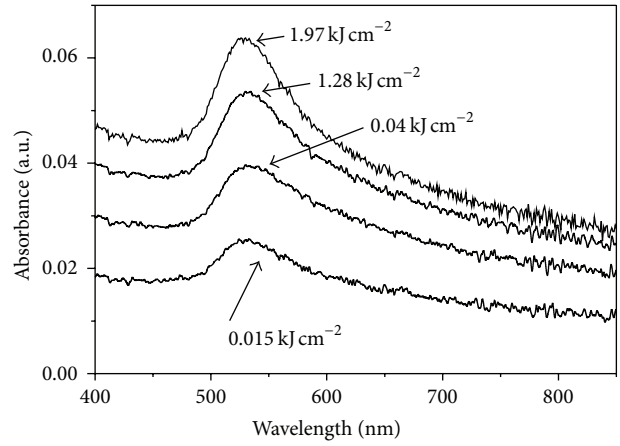

FIGURE 23: Absorbance spectra of gold suspensions at several surface energy densities. The laser pulse energy on the target was 75 mJ.

Note that 60 min of irradiation using the long pulses was needed in order to reach the same absorbance as obtained by 3 min of short pulse irradiation. Longer pulses decrease the production yields. Another observation was that the particles size distribution obtained using long pulses was narrower than that obtained using the short pulses. This can be attributed to the fact that at the long pulses the energy flux is lower, which allows for local equilibration, thus preventing extreme events that might result in very small or very large particles.

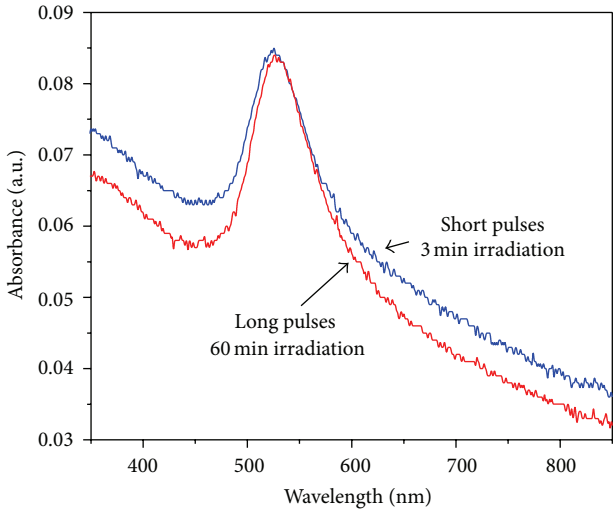

Figure 24: Absorbance spectra of gold nanoparticles in water, generated by short (6 ns) and long (120 μs) laser pulses. Note that much longer irradiation time (60 min) was needed using the long pulses, in order to obtain an absorbance similar to that obtained from short pulses.

The above results indicate that pulsed laser ablation of metals (e.g., silver and gold) in water enables synthesis of a variety of highly pure nanoparticles that can be integrated as functional components into sensors and different materials. The size and shape of the generated nanoparticles were found to be affected by illumination parameters (focusing lens, pulse energy, and duration).

7. Conclusions and Future Directions

Breakdown in colloidal suspensions is of considerable interest, both due to its scientific importance and due to its potential applications in chemical analysis of liquids. Since the atmosphere is rich in a large variety of aerosols at high concentrations, it comes out that all liquids exposed to air are actually suspensions. Therefore, breakdown in liquids should be almost always treated as breakdown in suspensions. The main consequence is that these breakdown events are of discrete nature and they are mainly governed by the nature of particulates.

The discrete nature of the breakdown and the crucial effects of the persistent particulates were not always understood. This was only recently proven, when high temporal and spatial measurements were performed using interferometric techniques. These measurements provided insight into the microstructure of the breakdown and into its dynamic processes, starting from the first few nanoseconds and up to the millisecond range. The differences in the behavior of various liquids could be explained in terms of the differences in their physical properties. The origin of the cylindrical shockwaves observed in some liquids and the way they are generated from merging of spherical individual events was thus revealed. Understanding the nature of the breakdown in liquids allowed for a new definition of their energy threshold. While old definitions were based on statistical measurements, recent studies suggested a definition based on simple measurements of the spark column lengths.

Understanding breakdown in liquids is also of considerable practical value. It can contribute to better analytical applications of this phenomenon. The limitations of the related analytical method in liquids are now clear and possible solutions have been suggested. While the performance of LIBS in liquids is still inferior, application of multivariate analysis methods has the potential to succeed in classifying suspended materials.

Besides the important application to LIBS analysis, optical breakdown in liquids can also be utilized for generation of suspended nanoparticles. This process is of importance in development of new sensors and various functional components. It was found that the size and shape of the suspended nanoparticles can be controlled by the laser irradiation characteristics, such as pulse energy, pulse duration, and focusing conditions.

It seems that further investigations are still needed. Clearly, temporal and spatial information on multipulse events is of great potential. So far, the powerful interferometric methods were only applied for single-pulse events, while it is well known that multiple pulses provide better LIBS performance in liquids. Note that although the signals are commonly integrated over many pulses, these experiments are still called single-pulse measurements, because all breakdowns were individual events. In contrast, in multipulse experiments pulses are temporally and spatially correlated. In a multipulse event in water suspension, the plasmas are generated in the microenvironment created by the previous pulses. In these cases, the shockwave dynamics described above are no longer valid. Interferometric visualization of the plasma evolution in multipulse events is expected to provide insight into the breakdown processes, which might result in better LIBS performance.

An additional promising research direction is the detailed understanding of the effects of the chemical properties of individual inclusion particulates upon the induced breakdown. Currently, only integrated results are obtained and one can speculate that some of the observed signal fluctuations are attributed to variations in the properties of the particulates. Therefore, understanding of these effects might result in better signal to noise ratios.

Breakdown on solid surfaces in water was also shown to be instrumental for fabrication of nanoparticles. So far, single-pulse measurements were performed and it has been shown that the properties of the suspended nanoparticles can be controlled by the irradiation parameters. One can envision new multipulse experiments, where the breakdowns are carried out in the microenvironment of the previous events. Under such experimental conditions, the dynamics are expected to be different and will probably result in different characteristics of the nanoparticles. Consider, for example, a sequence of pulses, controlled in time and phase, hitting the same surface site. This might provide much better control over the ablation processes and the resulting nanoparticle characteristics.

Another research of considerable interest is the optical breakdown in microsuspensions of various chemical compositions, for their fragmentation into nanoparticles. It has been shown that breakdown in suspensions is of discrete nature and it occurs at the inclusions. The fate of these inclusions has not been investigated yet. One can expect that the result would be an explosion of the microparticles and their fragmentation into nanoparticles. The resulting size distribution and the parameters that allow controlling the outcome of such microexplosions are still to be investigated.

Conflict of Interests

The authors declare that there is no conflict of interests regarding the publication of this paper.

References

[1] S. Yariv and H. Gross, *Geochemistry of Colloid Systems for Earth Scientists*, Springer, Berlin, Germany, 1979.

[2] D. Shaw, *Introduction to Colloid and Surface Chemistry*, Butterworth-Heinemann, London, UK, 1980.

[3] T. Wagner, T. Bundschuh, R. Schick, T. Schwartz, and R. Köster, "Investigation of colloidal water content with laser-induced breakdown detection during drinking water purification," *Acta Hydrochimica et Hydrobiologica*, vol. 30, no. 5-6, pp. 266–274, 2003.

[4] J. N. Ryan and M. Elimelech, "Colloid mobilization and transport in groundwater," *Colloids and Surfaces A: Physicochemical and Engineering Aspects*, vol. 107, pp. 1–56, 1996.

[5] M. Plaschke, T. Schäfer, T. Bundschuh et al., "Size characterization of bentonite colloids by different methods," *Analytical Chemistry*, vol. 73, no. 17, pp. 4338–4347, 2001.

[6] D. Cremers and L. Radziemski, *Handbook of Laser Induced Breakdown Spectroscopy*, Wiley, New York, NY, USA, 2006.

[7] D. Mukherjee, A. Rai, and M. R. Zachariah, "Quantitative laser-induced breakdown spectroscopy for aerosols via internal calibration: application to the oxidative coating of aluminum nanoparticles," *Journal of Aerosol Science*, vol. 37, no. 6, pp. 677–695, 2006.

[8] Ş. Yalçin, D. R. Crosley, G. P. Smith, and G. W. Faris, "Influence of ambient conditions on the laser air spark," *Applied Physics B: Lasers and Optics*, vol. 68, no. 1, pp. 121–130, 1999.

[9] D. E. Kim, K. J. Yoo, H. K. Park, K. J. Oh, and D. W. Kim, "Quantitative analysis of aluminum impurities in zinc alloy by laser-induced breakdown spectroscopy," *Applied Spectroscopy*, vol. 51, no. 1, pp. 22–29, 1997.

[10] M. Martin and M.-D. Cheng, "Detection of chromium aerosol using time-resolved laser-induced plasma spectroscopy," *Applied Spectroscopy*, vol. 54, no. 9, pp. 1279–1285, 2000.

[11] I. Schechter, "Direct aerosol analysis by time resolved laser plasma spectroscopy—improvement by single shot measurements," *Journal of Analytical Science and Technology*, vol. 8, pp. 779–786, 1995.

[12] T. Bundschuh, T. U. Wagner, and R. Köster, "Laser-induced Breakdown Detection (LIBD) for the highly sensitive quantification of aquatic colloids. Part I: Principle of LIBD and mathematical model," *Particle and Particle Systems Characterization*, vol. 22, no. 3, pp. 172–180, 2005.

[13] H. G. Barth and R. B. Flippen, "Particle size analysis," *Analytical Chemistry*, vol. 67, no. 12, pp. 257–272, 1995.

[14] F. J. Scherbaum, R. Knopp, and J. I. Kim, "Counting of particles in aqueous solutions by laser-induced photoacoustic breakdown detection," *Applied Physics B*, vol. 63, no. 3, pp. 299–306, 1996.

[15] C. Walther, S. Büchner, M. Filella, and V. Chanudet, "Probing particle size distributions in natural surface waters from 15 nm to 2 μm by a combination of LIBD and single-particle counting," *Journal of Colloid and Interface Science*, vol. 301, no. 2, pp. 532–537, 2006.

[16] T. Bundschuh, R. Knopp, and J. I. Kim, "Laser-induced breakdown detection (LIBD) of aquatic colloids with different laser systems," *Colloids and Surfaces A: Physicochemical and Engineering Aspects*, vol. 177, no. 1, pp. 47–55, 2001.

[17] R. Kaegi, T. Wagner, B. Hetzer, B. Sinnet, G. Tzvetkov, and M. Boller, "Size, number and chemical composition of nanosized particles in drinking water determined by analytical microscopy and LIBD," *Water Research*, vol. 42, no. 10-11, pp. 2778–2786, 2008.

[18] E. Damon and R. Thomlinson, "Observation of ionization of gases by a ruby laser," *Applied Optics*, vol. 2, no. 5, pp. 546–547, 1963.

[19] G. Weyl, *Physics of Laser-Induced Breakdown*, Marcel Dekker, New York, NY, USA, 1989.

[20] Y. P. Raizer, *Laser-Induced Discharge Phenomena*, Consultants Bureau, New York, NY, USA, 1977.

[21] J. R. Bettis, "Correlation among the laser-induced breakdown thresholds in solids, liquids, and gases," *Applied Optics*, vol. 31, no. 18, p. 3448, 1992.

[22] A. Alcock, C. DeMichelis, K. Hamal, and B. Tozer, "Expansion mechanism in a laser-produced spark," *Physical Review Letters*, vol. 20, no. 20, pp. 1095–1097, 1968.

[23] P. Chan and C. Lee, "Holographic schlieren investigation of laser-induced plasmas," *Physics Letters A*, vol. 62, no. 1, pp. 33–35, 1977.

[24] C. E. Bell and J. A. Landt, "Laser-induced high-pressure shock waves in water," *Applied Physics Letters*, vol. 10, no. 2, p. 46, 1967.

[25] M. P. Felix and A. T. Ellis, "Laser–induced liquid breakdown-a step-by-step account," *Applied Physics Letters*, vol. 19, no. 11, p. 484, 1971.

[26] W. Lauterborn and K. J. Ebeling, "High-speed holography of laser-induced breakdown in liquids," *Applied Physics Letters*, vol. 31, no. 10, pp. 663–664, 1977.

[27] F. Docchio, P. Regondi, M. R. C. Capon, and J. Mellerio, "Study of the temporal and spatial dynamics of plasmas induced in liquids by nanosecond Nd:YAG laser pulses 1: analysis of the plasma starting times," *Applied Optics*, vol. 27, no. 17, pp. 3661–3668, 1988.

[28] A. Vogel, K. Nahen, D. Theisen, and J. Noack, "Plasma formation in water by picosecond and nanosecond Nd:YAG laser pulses—part I: optical breakdown at threshold and superthreshold irradiance," *IEEE Journal on Selected Topics in Quantum Electronics*, vol. 2, no. 4, pp. 847–859, 1996.

[29] V. Bulatov, R. Krasniker, and I. Schechter, "Study of matrix effects in laser plasma spectroscopy by combined multifiber spatial and temporal resolutions," *Analytical Chemistry*, vol. 70, no. 24, pp. 5302–5311, 1998.

[30] I. Schechter and V. Bulatov, "Plasma morphology," in *LIBS—Fundamentals and Applications*, A. Miziolek, V. Palleschi, and I. Schechter, Eds., Cambridge University Press, Cambridge, Mass, USA, 2007.

[31] E. N. Glezer, C. B. Schaffer, N. Nishimura, and E. Mazur, "Minimally disruptive laser-induced breakdown in water," *Optics Letters*, vol. 22, no. 23, pp. 1817–1819, 1997.

[32] B. Zysset, J. G. Fujimoto, and T. F. Deutsch, "Time-resolved measurements of picosecond optical breakdown," *Applied Physics B Photophysics and Laser Chemistry*, vol. 48, no. 2, pp. 139–147, 1989.

[33] C. Vest, *Holographic Interferometry*, John Wiley & Sons, 1979.

[34] J. N. Butters, *Holography and Its Technology*, Peter Peregrinus, 1971.

[35] P. Hariharan, *Optical Holography*, Cambridge University Press, Cambridge,UK, 1984.

[36] P. Hariharan, *Basics of Interferometry*, Academic Press, New York, NY, USA, 1992.

[37] P. Hariharan, *Optical Interferometry*, Academic Press, 1985.

[38] T. Kreis, *Holographic Interferometry Principles and Methods*, Akademie Verlag, Berlin, Germany, 1996.

[39] R. Collier, C. Burckhardt, and L. Lin, *Optical Holography*, Academic Press, 1971.

[40] L. Bergmann and C. Schaefer, *Optics of Waves and Particles*, Walter de Gruyter, 1999.

[41] E. Hecht, *Optics*, Addison-Wesley, 1998.

[42] M. Born and E. Wolf, *Principles of Optics*, Cambridge University Press, Cambridge,UK, 1999.

[43] V. Venugopalan, A. Guerra III, K. Nahen, and A. Vogel, "Role of laser-induced plasma formation in pulsed cellular microsurgery and micromanipulation," *Physical Review Letters*, vol. 88, Article ID 078103, 2002.

[44] A. Vogel and V. Venugopalan, "Mechanisms of pulsed laser ablation of biological tissues," *Chemical Reviews*, vol. 103, no. 2, pp. 577–644, 2003.

[45] C. R. Phipps, *Laser Ablation and Its Applications*, Springer, Berlin, Germany, 2007.

[46] R. E. Russo, X. Mao, H. Liu, J. Gonzalez, and S. S. Mao, "Laser ablation in analytical chemistry—a review," *Talanta*, vol. 57, no. 3, pp. 425–451, 2002.

[47] V. Bulatov, R. Krasniker, and I. Schechter, "Converting spatial to pseudotemporal resolution in laser plasma analysis by simultaneous multifiber spectroscopy," *Analytical Chemistry*, vol. 72, no. 13, pp. 2987–2994, 2000.

[48] B. Dolgin, Y. Chen, V. Bulatov, and I. Schechter, "Use of LIBS for rapid characterization of parchment," *Analytical and Bioanalytical Chemistry*, vol. 386, no. 5, pp. 1535–1541, 2006.

[49] I. Schechter, "Laser induced plasma spectroscopy: a review of recent advances," *Reviews in Analytical Chemistry*, vol. 16, no. 3, pp. 173–298, 1997.

[50] A. Miziolek, V. Palleschi, and I. Schechter, Eds., *LIBS—Fundamentals and Applications*, Cambridge University Press, Cambridge, UK, 2007.

[51] V. Bulatov, L. Xu, and I. Schechter, "Spectroscopis imaging of laser-induced plasma," *Analytical Chemistry*, vol. 68, no. 17, pp. 2966–2973, 1996.

[52] R. Krasniker, V. Bulatov, and I. Schechter, "Study of matrix effects in laser plasma spectroscopy by shock wave propagation," *Spectrochimica Acta*, vol. 56, no. 6, pp. 609–618, 2001.

[53] V. Bulatov, A. Khalmanov, and I. Schechter, "Study of the morphology of a laser-produced aerosol plume by cavity ringdown laser absorption spectroscopy," *Analytical and Bioanalytical Chemistry*, vol. 375, no. 8, pp. 1282–1286, 2003.

[54] Y. Chen, V. Bulatov, L. Singer, J. Stricker, and I. Schechter, "Mapping and elemental fractionation of aerosols generated by laser-induced breakdown ablation," *Analytical and Bioanalytical Chemistry*, vol. 383, no. 7-8, pp. 1090–1097, 2005.

[55] G. A. Askaryan, A. M. Prokhorov, G. F. Chanturiya, and G. P. Shipulo, "The effects of a laser beam in a liquid," *Soviet Physics—JETP*, vol. 17, pp. 1463–1465, 1963.

[56] R. Brewer and K. Riekhoff, "Stimulated Brillouin scattering in liquids," *Physical Review Letters*, vol. 13, no. 11, pp. 334–336, 1964.

[57] E. F. Carome, C. E. Moeller, and N. A. Clark, "Intense ruby-laser-induced acoustic impulses in liquids," *The Journal of the Acoustical Society of America*, vol. 40, no. 6, p. 1462, 1966.

[58] L. C. Yang and V. J. Menichelli, "Detonation of insensitive high explosives by a Q−switched ruby laser," *Applied Physics Letters*, vol. 19, no. 11, p. 473, 1971.

[59] V. S. Teslenko, "Initial stage of extended laser breakdown in liquids," *IEEE Transactions on Electrical Insulation*, vol. 26, no. 6, pp. 1195–1200, 1991.

[60] F. Haruhisa, Y. Katsumi, and I. Yosio, in *Proceedings of the 6th International Conference on Conduction and Breakdown in Dielectric Liquids*, p. 247, Frontiers, Dreux, France, 1978.

[61] O. Martynenko, N. Stolovich, G. Rudinand, and S. Levchenko, in *Proceedings of the 8th ICOGER*, p. 64, Minsk, Belarus, 1981.

[62] N. Melikechi, H. Ding, O. A. Marcano, and S. Rock, "Laser-induced breakdown spectroscopy of alcohols and protein solutions," in *Proceedings of the 6th Ibero−American Conference on Optics (RIAO); 9th Latin-American Meeting on Optics, Lasers and Applications*, vol. 992 of *AIP Conference Proceedings*, pp. 1177–1182, 2008.

[63] A. Vogel, S. Busch, and U. Parlitz, "Shock wave emission and cavitation bubble generation by picosecond and nanosecond optical breakdown in water," *The Journal of the Acoustical Society of America*, vol. 100, no. 1, pp. 148–165, 1996.

[64] J. Noack and A. Vogel, "Single-shot spatially resolved characterization of laser-induced shock waves in water," *Applied Optics*, vol. 37, no. 19, pp. 4092–4099, 1998.

[65] A. Vogel, N. Linz, S. Freidank, and G. Paltauf, "Femtosecond-laser-induced nanocavitation in water: implications for optical breakdown threshold and cell surgery," *Physical Review Letters*, vol. 100, Article ID 038102, 2008.

[66] F. Docchio, "Lifetimes of plasmas induced in liquids and ocular media by single Nd:YAG laser pulses of different duration," *Europhysics Letters*, vol. 6, p. 407, 1988.

[67] A. Vogel, J. Noack, D. Theisen et al., "Energy balance of optical breakdown in water at nanosecond to femtosecond time scales," *Applied Physics B: Lasers and Optics*, vol. 68, no. 2, pp. 271–280, 1999.

[68] E.-A. Brujan and A. Vogel, "Stress wave emission and cavitation bubble dynamics by nanosecond optical breakdown in a tissue phantom," *Journal of Fluid Mechanics*, vol. 558, pp. 281–308, 2006.

[69] Y. Yasojima, "Experimental studies on breakdown probability in liquids by nanoseconds laser," *Kinki Daigaku Kogakubu Kenkyu Hokoku*, vol. 41, p. 65, 2007.

[70] Y. Yasojima, "Optical field dependence of breakdown in liquids by Q-switched lasers," in *Proceedings of the IEEE 15th International Conference on Dielectric Liquids (ICDL '05)*, vol. 67, pp. 67–70, Coimbra, Portugal, July 2005.

[71] G. Toker, V. Bulatov, T. Kovalchuk, and I. Schechter, "Microdynamics of optical breakdown in water induced by nanosecond laser pulses of 1064 nm wavelength," *Chemical Physics Letters*, vol. 471, no. 4–6, pp. 244–248, 2009.

[72] T. Kovalchuk, G. Toker, V. Bulatov, and I. Schechter, "Laser breakdown in alcohols and water induced by $\lambda = 1064$ nm nanosecond pulses," *Chemical Physics Letters*, vol. 500, no. 4–6, pp. 242–250, 2010.

[73] H. Young, R. Freedman, T. Sandin, and A. Ford, *Sears and Zemansky's University Physics*, Section 11-6, Addison-Wesley, 10th edition, 1999.

[74] A. Vogel and J. Noack, "Shock-wave energy and acoustic energy dissipation after laser-induced breakdown," in *Laser Tissue Interaction IX*, vol. 3254 of *Proceedings of SPIE*, p. 180, 1998.

[75] A. Vogel and W. Lauterborn, "Acoustic transient generation by laser–produced cavitation bubbles near solid boundaries," *The Journal of the Acoustical Society of America*, vol. 84, p. 719, 1988.

[76] L. I. Sedov, *Similarity and Dimensional Methods in Mechanics*, Mir Publishers, Moscow, Russia, 1982.

[77] P. K. Kennedy, D. X. Hammer, and B. A. Rockwell, "Laser-induced breakdown in aqueous media," *Progress in Quantum Electronics*, vol. 21, no. 3, pp. 155–248, 1997.

[78] T. Bundschuh, T. U. Wagner, and R. Köster, "Laser-induced breakdown detection (LIBD) for the highly sensitive quantification of aquatic colloids. Part I: principle of LIBD and mathematical model," *Particle & Particle Systems Characterization*, vol. 22, no. 3, pp. 172–180, 2005.

[79] Y. Zeldovich and Y. Raizer, *Physics of Shock Waves and High-Temperature Hydrodynamic Phenomena*, vol. 1, Academic Press, New York, NY, USA, 1966.

[80] J.-P. Sylvestre, A. V. Kabashin, E. Sacher, and M. Meunier, "Femtosecond laser ablation of gold in water: influence of the laser-produced plasma on the nanoparticle size distribution," *Applied Physics A*, vol. 80, no. 4, pp. 753–758, 2005.

[81] D. Lide, *Physical Constants of Organic Compounds*, CRC Press, Boca Raton, Fla, USA, 2005.

[82] A. S. Eppler, D. A. Cremers, D. D. Hickmott, M. J. Ferris, and A. C. Koskelo, "Matrix effects in the detection of Pb and Ba in soils using laser-induced breakdown spectroscopy," *Applied Spectroscopy*, vol. 50, no. 9, pp. 1175–1181, 1996.

[83] B. Charfi and M. A. Harith, "Panoramic laser-induced breakdown spectrometry of water," *Spectrochimica Acta Part B: Atomic Spectroscopy*, vol. 57, no. 7, pp. 1141–1153, 2002.

[84] M. A. Gondal, T. Hussain, and Z. H. Yamani, "Optimization of the LIBS parameters for detection of trace metals in petroleum products," *Energy Sources A*, vol. 30, no. 5, pp. 441–451, 2008.

[85] K. Y. Yamamoto, D. A. Cremers, L. E. Foster, M. P. Davies, and R. D. Harris, "Laser-induced breakdown spectroscopy analysis of solids using a long-pulse (150 ns) Q-switched Nd:YAG laser," *Applied Spectroscopy*, vol. 59, no. 9, pp. 1082–1097, 2005.

[86] R. Wisbrun, I. Schechter, R. Niessner, H. Schröder, and K. L. Kompa, "Detector for trace elemental analysis of solid environmental samples by laser plasma spectroscopy," *Analytical Chemistry*, vol. 66, no. 18, pp. 2964–2975, 1994.

[87] L. M. Cabalín and J. J. Laserna, "Experimental determination of laser induced breakdown thresholds of metals under nanosecond Q-switched laser operation," *Spectrochimica Acta Part B: Atomic Spectroscopy*, vol. 53, no. 5, pp. 723–730, 1998.

[88] L. J. Radziemski and T. R. Loree, "Laser-induced breakdown spectroscopy: time-resolved spectrochemical applications," *Plasma Chemistry and Plasma Processing*, vol. 1, no. 3, pp. 281–293, 1981.

[89] L. Dudragne, P. Adam, and J. Amouroux, "Time-resolved laser-induced breakdown spectroscopy: application for qualitative and quantitative detection of fluorine, chlorine, sulfur, and carbon in air," *Applied Spectroscopy*, vol. 52, no. 10, pp. 1321–1327, 1998.

[90] J. R. Wachter and D. A. Cremers, "Determination of uranium in solution using laser-induced breakdown spectroscopy," *Applied Spectroscopy*, vol. 41, no. 6, pp. 1042–1048, 1987.

[91] L. Xu and I. Schechter, "Wavelength selection for simultaneous spectroscopic analysis. Experimental and theoretical study," *Analytical Chemistry*, vol. 68, no. 14, pp. 2392–2400, 1996.

[92] I. Litani-Barzilai and I. Schechter, "Spectroscopic prediction of nonlinear properties by principal component regression," *Analytica Chimica Acta*, vol. 348, no. 1–3, pp. 345–356, 1997.

[93] L. Xu and I. Schechter, "A calibration method free of optimum factor number selection for automated multivariate analysis. Experimental and theoretical study," *Analytical Chemistry*, vol. 69, no. 18, pp. 3722–3730, 1997.

[94] R. Barbini, F. Colao, R. Fantoni et al., "Semi-quantitative time resolved LIBS measurements," *Applied Physics B: Lasers and Optics*, vol. 65, no. 1, pp. 101–107, 1997.

[95] L. Xu, V. Bulatov, V. V. Gridin, and I. Schechter, "Absolute analysis of particulate materials by laser-induced breakdown spectroscopy," *Analytical Chemistry*, vol. 69, no. 11, pp. 2103–2108, 1997.

[96] M. Z. Martin, N. Labbé, T. G. Rials, and S. D. Wullschleger, "Analysis of preservative-treated wood by multivariate analysis of laser-induced breakdown spectroscopy spectra," *Spectrochimica Acta Part B: Atomic Spectroscopy*, vol. 60, no. 7-8, pp. 1179–1185, 2005.

[97] N. Labbé, I. M. Swamidoss, N. André, M. Z. Martin, T. M. Young, and T. G. Rials, "Extraction of information from laser-induced breakdown spectroscopy spectral data by multivariate analysis," *Applied Optics*, vol. 47, no. 31, pp. G158–G165, 2008.

[98] M. Z. Martin, N. Labbé, N. André et al., "High resolution applications of laser-induced breakdown spectroscopy for environmental and forensic applications," *Spectrochimica Acta Part B: Atomic Spectroscopy*, vol. 62, no. 12, pp. 1426–1432, 2007.

[99] B. Bousquet, J.-B. Sirven, and L. Canioni, "Towards quantitative laser-induced breakdown spectroscopy analysis of soil samples," *Spectrochimica Acta Part B: Atomic Spectroscopy*, vol. 62, no. 12, pp. 1582–1589, 2007.

[100] R. Gaudiuso, M. Dell'Aglio, O. de Pascale, G. S. Senesi, and A. de Giacomo, "Laser induced breakdown spectroscopy for elemental analysis in environmental, cultural heritage and space applications: a review of methods and results," *Sensors*, vol. 10, no. 8, pp. 7434–7468, 2010.

[101] I. Schechter, R. Wisbrun, R. Nießner, H. Schröder, and K. L. Kompa, "Signal processing algorithm for simultaneous multi-element analysis by laser-produced plasma spectroscopy," in *International Society for Optical Engineering*, vol. 2093 of *Proceedings of SPIE*, 1994, pp. 310–321.

[102] R. Knopp, F. J. Scherbaum, and J. I. Kim, "Laser Induced Breakdown Spectroscopy (LIBS) as an analytical tool for the detection of metal ions in aqueous solutions," *Fresenius' Journal of Analytical Chemistry*, vol. 355, no. 1, pp. 16–20, 1996.

[103] Y. Ito, O. Ueki, and S. Nakamura, "Determination of colloidal iron in water by laser-induced breakdown spectroscopy," *Analytica Chimica Acta*, vol. 299, no. 3, pp. 401–405, 1995.

[104] M. Adamson, A. Padmanabhan, G. J. Godfrey, and S. J. Rehse, "Laser-induced breakdown spectroscopy at a water/gas interface: a study of bath gas-dependent molecular species," *Spectrochimica Acta Part B: Atomic Spectroscopy*, vol. 62, no. 12, pp. 1348–1360, 2007.

[105] L. Xu, V. Bulatov, V. V. Gridin, and I. Schechter, "Absolute analysis of particulate materials by laser-induced breakdown spectroscopy," *Analytical Chemistry*, vol. 69, no. 11, pp. 2103–2108, 1997.

[106] J. E. Carranza, B. T. Fisher, G. D. Yoder, and D. W. Hahn, "On-line analysis of ambient air aerosols using laser-induced breakdown spectroscopy," *Spectrochimica Acta Part B: Atomic Spectroscopy*, vol. 56, no. 6, pp. 851–864, 2001.

[107] K. Y. Yamamoto, D. A. Cremers, M. J. Ferris, and L. E. Foster, "Detection of metals in the environment using a portable laser-induced breakdown spectroscopy instrument," *Applied Spectroscopy*, vol. 50, no. 2, pp. 222–233, 1996.

[108] J.-B. Sirven, B. Bousquet, L. Canioni, and L. Sarger, "Laser-induced breakdown spectroscopy of composite samples: comparison of advanced chemometrics methods," *Analytical Chemistry*, vol. 78, no. 5, pp. 1462–1469, 2006.

[109] F. C. de Lucia Jr., J. L. Gottfried, C. A. Munson, and A. W. Miziolek, "Multlvariate analysis of standoff laser-induced breakdown spectroscopy spectra for classification of explosive-containing residues," *Applied Optics*, vol. 47, no. 31, pp. G112–G122, 2008.

[110] R. Wisbrun, I. Schechter, R. Nießner, and H. Schröder, "Laser-induced breakdown spectroscopy for detection of heavy metals in environmental samples," in *International Conference on Monitoring of Toxic Chemicals and Biomarkers*, vol. 1716 of *Proceedings of SPIE*, March 1993.

[111] I. Schechter, R. Wisbrun, R. Nießner, H. Schröder, and K. L. Kompa, "Real-time detection of hazardous elements in sand and soils," in *Substance Detection Systems*, vol. 2092 of *Proceedings of SPIE*, pp. 174–185, International Society of Optical Engineering, March 1994.

[112] I. Schechter, V. Bulatov, L. Xu, V. V. Gridin, and R. Krasniker, "Improved laser-induced-breakdown analysis of environmental samples by plasma imaging," *Trends in Optics and Photonics*, vol. 36, pp. 178–180, 2000.

[113] H. Schröder, I. Schechter, R. Wisbrun, and R. Nießner, "Detection of heavy metals in environmental samples using laser spark analysis," in *Excimer Lasers: The Tools, Fundamentals of Their Interactions with Matter, Fields of Applications*, L. D. Laude, Ed., pp. 269–287, Kluwer Academic Publishers, Boston, Mass, USA, 1994.

[114] J. L. Gottfried, R. S. Harmon, F. C. de Lucia Jr., and A. W. Miziolek, "Multivariate analysis of laser-induced breakdown spectroscopy chemical signatures for geomaterial classification," *Spectrochimica Acta—Part B Atomic Spectroscopy*, vol. 64, no. 10, pp. 1009–1019, 2009.

[115] A. C. Samuels, F. C. DeLucia Jr., K. L. McNesby, and A. W. Miziolek, "Laser-induced breakdown spectroscopy of bacterial spores, molds, pollens, and protein: initial studies of discrimination potential," *Applied Optics*, vol. 42, no. 30, pp. 6205–6209, 2003.

[116] A. Sarkar, D. Alamelu, and S. K. Aggarwal, "Determination of thorium and uranium in solution by laser-induced breakdown spectrometry," *Applied Optics*, vol. 47, no. 31, pp. G58–G64, 2008.

[117] A. Sarkar, S. K. Aggarwal, K. Sasibhusan, and D. Alamelu, "Determination of sub-ppm levels of boron in ground water samples by laser induced breakdown spectroscopy," *Microchimica Acta*, vol. 168, no. 1-2, pp. 65–69, 2010.

[118] A. R. Boyain-Goitia, D. C. S. Beddows, B. C. Griffiths, and H. H. Telle, "Single-pollen analysis by laser-induced breakdown spectroscopy and raman microscopy," *Applied Optics*, vol. 42, no. 30, pp. 6119–6132, 2003.

[119] M. Yao, J. Lin, M. Liu, Q. Li, and Z. Lei, in *Proceedings of the 3rd International Conference on Biomedical Engineering and Informatics (BMEI '10)*, Yantai, China, October 2010.

[120] C. A. Porcelli, F. H. Gutierrez Boem, and R. S. Lavado, "The K/Na and Ca/Na ratios and rapeseed yield, under soil salinity or sodicity," *Plant and Soil*, vol. 175, no. 2, pp. 251–255, 1995.

[121] M. A. Khan, M. U. Shirazi, S. M. Mujtaba et al., "Role of proline, K/NA ratio and chlorophyll content in salt tolerance of wheat (*Triticum aestivum* L.)," *Pakistan Journal of Botany*, vol. 41, no. 2, pp. 633–638, 2009.

[122] F. C. De Lucia Jr., J. L. Gottfried, C. A. Munson, and A. W. Miziolek, "Multlvariate analysis of standoff laser-induced breakdown spectroscopy spectra for classification of explosive-containing residues," *Applied Optics*, vol. 47, no. 31, pp. G112–G122, 2008.

[123] A. Kumar, F.-Y. Yueh, J. P. Singh, and S. Burgess, "Characterization of malignant tissue cells by laser-induced breakdown spectroscopy," *Applied Optics*, vol. 43, no. 28, pp. 5399–5403, 2004.

[124] T. E. Fox, E. G. H. M. van den Heuvel, C. A. Atherton et al., "Biovailability of selenium from fish, yeast and selenate: a comparative study in humans using stable isotopes," *European Journal of Clinical Nutrition*, vol. 58, no. 2, pp. 343–349, 2004.

[125] K. Okamoto and K. Fuwa, "Preparation and certification of tea leaves reference material," *Fresenius' Zeitschrift für Analytische Chemie*, vol. 326, no. 7, pp. 622–626, 1987.

[126] R. Giulian, C. E. I. dos Santos, S. de Moraes Shubeita, L. M. da Silva, J. F. Dias, and M. L. Yoneama, "Elemental characterization of commercial mate tea leaves (*Ilex paraguariensis* A. St.-Hil.) before and after hot water infusion using ion beam techniques," *Journal of Agricultural and Food Chemistry*, vol. 55, no. 3, pp. 741–746, 2007.

[127] S. Barcikowski, F. Devesa, and K. Moldenhauer, "Impact and structure of literature on nanoparticle generation by laser ablation in liquids," *Journal of Nanoparticle Research*, vol. 11, no. 8, pp. 1883–1893, 2009.

[128] G. W. Yang, "Laser ablation in liquids: applications in the synthesis of nanocrystals," *Progress in Materials Science*, vol. 52, no. 4, pp. 648–698, 2007.

[129] B. Khlebtsov, V. Zharov, A. Melnikov, V. Tuchin, and N. Khlebtsov, "Optical amplification of photothermal therapy with gold nanoparticles and nanoclusters," *Nanotechnology*, vol. 17, no. 20, pp. 5167–5179, 2006.

[130] T. A. Taton, C. A. Mirkin, and R. L. Letsinger, "Scanometric DNA array detection with nanoparticle probes," *Science*, vol. 289, no. 5485, pp. 1757–1760, 2000.

[131] G. Raschke, S. Kowarik, T. Franzl et al., "Biomolecular recognition based on single gold nanoparticle light scattering," *Nano Letters*, vol. 3, no. 7, pp. 935–938, 2003.

[132] S. Link and M. A. El-Sayed, "Size and temperature dependence of the plasmon absorption of colloidal gold nanoparticles," *The Journal of Physical Chemistry B*, vol. 103, no. 21, pp. 4212–4217, 1999.

[133] A. V. Kabashin and M. Meunier, "Femtosecond laser ablation in aqueous solutions: a novel method to synthesize non-toxic metal colloids with controllable size," *Journal of Physics: Conference Series*, vol. 59, article 354, 2007.

[134] B. C. Stuart, M. D. Feit, S. Herman, A. M. Rubenchik, B. W. Shore, and M. D. Perry, "Optical ablation by high-power short-pulse lasers," *Journal of the Optical Society of America B: Optical Physics*, vol. 13, no. 2, pp. 459–468, 1996.